

Hybrid Quantum/Classical Derivative Theory: Analytical Gradients and Excited-State Dynamics for the Multistate Contracted Variational Quantum Eigensolver

Robert M. Parrish,^{1,2,3,*} Edward G. Hohenstein,^{2,3} Peter L. McMahon,^{1,4} and Todd J. Martínez^{2,3}

¹ QC Ware Corporation, Palo Alto, CA 94301

² Department of Chemistry and the PULSE Institute, Stanford University, Stanford, CA 94305

³ SLAC National Accelerator Laboratory, Menlo Park, CA 94025

⁴ E. L. Ginzton Laboratory, Stanford University, Stanford, CA 94305

The maturation of analytical derivative theory over the past few decades has enabled classical electronic structure theory to provide accurate and efficient predictions of a wide variety of observable properties. However, classical implementations of analytical derivative theory take advantage of explicit computational access to the approximate electronic wavefunctions in question, which is not possible for the emerging case of hybrid quantum/classical methods. Here, we develop an efficient Lagrangian-based approach for analytical first derivatives of hybrid quantum/classical methods using only observable quantities from the quantum portion of the algorithm. Specifically, we construct the key first-derivative property of the nuclear energy gradient for the recently-developed multistate, contracted variant of the variational quantum eigensolver (MC-VQE) within the context of the *ab initio* exciton model (AIEM). We show that a clean separation between the quantum and classical parts of the problem is enabled by the definition of an appropriate set of relaxed density matrices, and show how the wavefunction response equations in the quantum part of the algorithm (coupled-perturbed MC-VQE or CP-MC-VQE equations) are decoupled from the wavefunction response equations and gradient perturbations in the classical part of the algorithm. We explore the magnitudes of the Hellmann-Feynman and response contributions to the gradients in quantum circuit simulations of MC-VQE+AIEM and demonstrate a quantum circuit simulator implementation of adiabatic excited state dynamics with MC-VQE+AIEM.

I. INTRODUCTION

The emergence of hybrid variational quantum/classical algorithms¹ for the approximate diagonalization of the electronic Hamiltonian represents a promising pathway to the robust and accurate determination of observable properties in strongly-correlated molecular systems on noisy intermediate-scale quantum (NISQ) hardware.² However, most efforts to this point have focused on ground-state^{1,3-8} and, more-recently, excited-state energies^{1,9-14} at a single nuclear geometry. To make further progress, efforts are needed to extend these methods to the efficient computation of analytical derivative properties such as nuclear energy gradients,¹⁵⁻²⁵ relaxed dipole moments,^{26,27} dipole derivatives,^{16,20,28} electronic polarizabilities,²⁹⁻³² polarizability derivatives,³³ circular dichroism spectra,³⁴⁻³⁶ nuclear magnetic resonance (NMR) shielding tensors,³⁷⁻⁴³ NMR spin-spin coupling constants,^{44,45} hyperfine coupling constants,⁴⁶ vibrational frequencies,^{17,20,47,48} and non-adiabatic coupling vectors.⁴⁹⁻⁵³ In attempting such extensions, we will have to contend with the fact that the hybrid quantum/classical methods generally utilize an approximate wavefunction ansatz and will therefore carry wavefunction response terms in the desired analytical derivative properties. The efficient computation of such analytical derivative properties using only the simple low-order Pauli expectation values that are available at the output of quantum circuits (i.e., without explicit knowledge of the many-electron wavefunctions) is the major focus of the present work. Specifically, we will focus on develop-

ing analytical nuclear gradients of our recently-developed multistate, contracted variant of the variational quantum eigensolver¹⁴ (MC-VQE) within the *ab initio* exciton model⁵⁴⁻⁵⁶ (AIEM) framework. MC-VQE provides a route to the balanced treatment of ground-state, excited-state and transition properties, and is the latest in an extensive series of methods proposed to extend VQE to accurately and efficiently handle excited states.^{1,9-13}

In the context of classical electronic structure theory, much progress has been made in the last few decades in the computation of accurate observable properties as analytical derivatives of expectation values of approximate electronic wavefunctions. As one key example, determining the analytical gradient of the adiabatic energy for a given electronic state with respect to the nuclear positions yields the classical forces acting on the nuclei at a given nuclear configuration and electronic state. This provides first-order Taylor series information of the potential energy surface for the electronic state, and allows for myriad applications that would be otherwise intractable with only energies.⁵⁷ For instance, gradient-based optimization of the energy with respect to nuclear coordinates yields local energy minima of the potential energy surface, which are useful proxies for the stable equilibrium geometries of molecular species. First-order saddle points on the potential energy surface can be located with similar gradient-based algorithms, yielding the transition state structures for interesting chemical reactions. Second-order derivatives of the energy with respect to the nuclear coordinates (Hessians) can be used at optimal structures to obtain a harmonic approxima-

tion for the nuclear wavepacket, including predictions of zero-point vibrational energy, finite-temperature vibrational enthalpy/entropy, and infrared and Raman spectra. Taken together, the first and second-order derivative properties at two minimal structures and the connecting transition state can provide an estimate of the reaction energy and a transition-state-theory estimate of the reaction rate.⁵⁸⁻⁶² Additionally, in the real time axis, analytical nuclear gradients can also be used to perform *ab initio* molecular dynamics (AIMD), which, in its simplest form, involves the classical Newtonian propagation of the nuclei along the Born-Oppenheimer electronic potential surface. Note that with efficient codes for the computation of the electronic energy and its analytical nuclear gradient at a given nuclear configuration, AIMD can be performed with “on-the-fly” sampling of the potential energy surface, allowing for its deployment in systems with thousands of atoms, e.g., no intractable grid-based representation of the potential surface is needed. AIMD is particularly useful for computing time-resolved observables of non-equilibrium chemical processes. Many extensions of AIMD have been developed to account for the fact that the nuclei are non-classical and/or to relax the Born-Oppenheimer approximation and target the full solution of the molecular Schrödinger equation - such methods include *ab initio* multiple spawning (AIMS),⁶³ fewest switches surface hopping (FSSH),⁶⁴ multi-configurational Ehrenfest (AI-MCE),⁶⁵ variational multiconfigurational Gaussian methods (vMCG),⁶⁶ and many variants. Aside from heavy reliance on the nuclear energy gradient, a critical derivative quantity encountered ubiquitously in AIMS and the other non-adiabatic dynamics methods is the “non-adiabatic coupling vector,” which determines how much the electronic overlap between two adiabatic states changes as one of the states is moved.⁴⁹⁻⁵³ The non-adiabatic coupling vector is usually formulated as a highly unusual derivative property that does not straightforwardly resemble an observable but nonetheless relies heavily on analytical derivative machinery - we will discuss the hybrid quantum/classical treatment of the non-adiabatic coupling vector in MC-VQE in a forthcoming companion paper.

In all of these applications, the practitioners of analytical gradient theory have developed two coupled governing principles:

1. Regardless of the origins or definitions of the approximate electronic wavefunction, one should always take the *exact* derivative of the approximated observable expectation value - no further approximations should be permitted in the derivative. This makes the derivative self-consistent with the approximated observable expectation value, which often provides for markedly favorable cancellation of errors in properties. In many cases, this principle is fundamentally required for practical use the derivative property: As one such instance, the gradient of the energy with respect to nuclear coordinates must be self-consistent with the approximate en-

ergy observable to allow for the equations of motion of *ab initio* molecular dynamics to be integrated while respecting the inviolable invariant of conservation of energy. Generally, satisfying this principle mandates the consideration of the derivatives of the approximations built into the wavefunction definitions with respect to gradient perturbations, a topic loosely known as “wavefunction response.”

2. With careful effort, it is generally possible to formulate first derivatives of arbitrary observable expectation values in a way that depends weakly (or ideally not at all) on the number of gradient perturbations. More concretely, it is generally possible to restructure the derivative problem in a way where the explicit wavefunction response does not need to be computed separately for each gradient perturbation - instead, an effective collective wavefunction response can be computed once and used in conjunction with the chain rule to efficiently compute the desired total derivatives. Often this leads to the ideal case where the computation of the analytical derivative property costs the *same* as the underlying observable, to within some constant prefactor.

Analytical derivative theory has a long and rich history in the electronic structure literature. Starting from the pioneering work by Pulay and others in the computation of the analytical gradient of approximate Hartree-Fock theory,¹⁵⁻¹⁷ it was immediately noticed that analytical derivative theory was plagued by extreme verbosity of the required equations, requiring careful efforts to produce correct derivatives (particularly those involving explicit wavefunction response terms). The explicit forward differentiation of the wavefunction response contributions was heavily developed during the 1980s in a style characterized by noteworthy contributions from Yamaguchi and Schaefer.⁶⁷ At around this time, a major breakthrough was realized in the widespread deployment of Handy-Schaefer *Z*-vector method⁶⁸ (also sometimes known as the “Delgarno-Stewart interchange theorem”⁶⁹), which removed the need to explicitly solve for the response of the wavefunction parameters to each gradient perturbation. The *Z*-vector method substantially accelerated analytical gradient theory, to the point that it was generally far superior to finite difference approximations in both runtime and accuracy, but was often seen as a clever mathematical/computational manipulation rather than a fundamental feature of analytical gradient theory. This changed with the widespread adoption of the Lagrangian formalism of Helgaker⁷⁰ for analytical derivatives of approximate wavefunctions in the late 1980s and early 1990s^{42,46,71-80} - the non-variational energy (or other observable) expression for a given approximate wavefunction method can be exchanged for an equivalent Lagrangian scalar quantity with additional Lagrange multiplier parameters. Making the Lagrangian variational with respect to the Lagrange multiplier parameters provides a succinct and rigorous definition of the usual

wavefunction parameters, while making the Lagrangian variational with respect to the usual wavefunction parameters determines the values of the Lagrange multiplier parameters through a series of linear “wavefunction response” equations. Notably, the Handy-Schaefer Z -vector method arises naturally in the Lagrangian formalism, automatically minimizing the number of wavefunction response equations that must be solved for a given observable (regardless of the number of derivative perturbations).

While there have been considerable recent efforts to develop hybrid quantum/classical methods for zeroth-order scalar observables such as ground-state and excited-state energies and transition properties, the existing literature on hybrid quantum/classical analytical derivative theory is notably sparse. An approach for the nuclear energy gradient (and higher derivatives) has been proposed⁸¹ based on Jordan’s quantum gradient estimation algorithm within the phase estimation algorithm. More recently, another approach has been proposed⁸² for linear response based on perturbations of the phase estimation algorithm. Within the original VQE method, it is also clear that the nuclear energy gradient of the ground state is straightforward to compute, as the variational density matrix is available as a byproduct of the VQE optimization.³ However, this approach will not be applicable to most excited state VQE extensions or to transition properties, as here the quantities to be differentiated are not variational in the quantum circuit parameters. Finally, as the numerical experiments in this manuscript were being finalized, two separate groups have proposed methodology for the computation of the nuclear energy gradient using a sum-over-states approach⁸³ and using an explicit differentiation approach.⁸⁴ Both groups demonstrate their method in the context of H_2 . Notably, no correspondence of the Handy-Schaefer Z -vector method or the Lagrangian formalism has yet been introduced - existing approaches either ignore the effect of wavefunction response or compute it through direct forward evaluation of the response derivatives⁸⁴ or effectively through a sum-over-states resolution.⁸³

In the present manuscript, we first review some technical prerequisites related to the Lagrangian formalism of analytical derivative theory and efficient/accurate techniques for computing the analytical gradients of quantum circuit observable expectation values with respect to circuit parameters. We then carefully define and differentiate each stage of the MC-VQE algorithm in the specific context of the AIEM. The expressions developed herein are deliberately specific to the AIEM to provide an impression of the flow of a Lagrangian workflow for hybrid quantum/classical derivative theory. However, the overall steps would be similar for other Hamiltonian representations, such as fermionic systems represented by the Jordan-Wigner,^{85,86} Bravyi-Kitaev,^{87,88} or other spin-lattice representations.^{89–93} Moreover, the general hybrid quantum/classical Lagrangian approach adopted herein should be straightforward to adapt to other vari-

ants of VQE. Finally, the broad sketches of the approach developed in this work should apply equally to other derivative properties such as non-adiabatic coupling vectors - in particular, the various response equations appearing here will be identical up to the choice of right-hand side.

II. TECHNICAL BACKGROUND

A. Analytical Derivative Theory

Analytical derivative theory is concerned with the computation of derivatives of expectation values of observable quantities of approximate wavefunctions,

$$d_\zeta O_\Theta \equiv d_\zeta \langle \Psi_\Theta | \hat{O} | \Psi_\Theta \rangle \quad (1)$$

Here d_ζ is shorthand for the total derivative $d/d\zeta$ (∂_ζ will similarly serve as shorthand for the partial derivative $\partial/\partial\zeta$). For instance, substituting $\hat{O} \equiv \hat{H}$ and taking ζ to be the Cartesian coordinates of the nuclei yields the traditional “energy gradient,” E^ζ which is equivalent to the opposite of the force acting on the nuclei at a given nuclear geometry. We will specialize to the case of the nuclear gradient in all derivations in the present manuscript. Analytical derivatives of other properties such as non-adiabatic coupling vectors, dipole derivatives, etc, would follow similar manipulations.

In general there are several contributions to the gradient,

$$d_\zeta E_\Theta = \langle \Psi_\Theta | d_\zeta \hat{H} | \Psi_\Theta \rangle + \langle \Psi_\Theta | \hat{H} | d_\zeta \Psi_\Theta \rangle + \text{H.C.} \quad (2)$$

The first term is the “Hellmann-Feynman” contribution,^{94–97} which reflects the expectation value of the intrinsic derivative of the Hamiltonian with respect to ζ . The last two terms are the “wavefunction response” contributions, which reflect the fact that the wavefunction parameters may vary with respect to ζ , providing an additional nonzero contribution to the gradient.

More explicitly, the wavefunction $|\Psi_\Theta\rangle$ might definitionally depend on a set of parameters $\{\theta_i\}$, which themselves depend on \hat{H} (or perhaps other operators), and from thence depend on ζ . E.g., $\{\theta_i\}$ might be determined by solving another electronic structure method involving implicit equations in \hat{H} . Therefore,

$$\frac{dE_\Theta(\hat{H}, \{\theta_i\})}{d\zeta} = \frac{\partial E_\Theta}{\partial \hat{H}} \frac{d\hat{H}}{d\zeta} + \frac{\partial E_\Theta}{\partial \theta_i} \frac{d\theta_i}{d\zeta} \quad (3)$$

The explicit computation of the wavefunction response over a large number of perturbation coordinates ζ may prove to be exhaustingly tedious.

The Lagrangian formalism⁷⁰ can help overcome this difficulty and reduce the number of wavefunction response contributions that must be considered. The Lagrangian formalism involves the replacement of the observable $E_\Theta(\hat{H}, \{\theta_i\})$ with an equivalent scalar quantity

$$\mathcal{L}_\Theta(\hat{H}, \{\theta_i\}, \{\tilde{\theta}_i\}),$$

$$\mathcal{L}_\Theta(\hat{H}, \{\theta_i\}, \{\tilde{\theta}_i\}) \equiv E_\Theta(\hat{H}, \{\theta_i\}) + \underbrace{\sum_i \tilde{\theta}_i f_i(\hat{H}, \{\theta_j\})}_0 \quad (4)$$

in such a way that the definitions of the wavefunction parameters $\{\theta_i\}$ are built into \mathcal{L}_Θ by Lagrange multipliers $\{\tilde{\theta}_i\}$. I.e., for each set of (generally nonlinear) equations $\{f_i(\hat{H}, \{\theta_j\}) = 0\}$ determining a class of wavefunction parameters $\{\theta_j\}$, a Lagrange multiplier term $\sum_i \tilde{\theta}_i f_i(\hat{H}, \{\theta_j\})$ is added into the Lagrangian \mathcal{L}_Θ . Making the Lagrangian stationary with respect to the Lagrange multiplier parameters $\{\tilde{\theta}_i\}$, e.g., $d_{\tilde{\theta}_i} \mathcal{L}_\Theta = 0$ provides the definition of the wavefunction parameters, e.g., $\Rightarrow \{f_i(\hat{H}, \{\theta_j\}) = 0\}$. Making the Lagrangian stationary with respect to the intrinsic wavefunction parameters $\{\theta_i\}$, e.g., $d_{\theta_j} \mathcal{L}_\Theta = 0$ determines the values of the Lagrange multipliers $\{\tilde{\theta}_j\}$ via the solution of a set of linear equations (the “response equations”). Once the response equations have been solved, the total gradient does not require the explicit determination of the parameter derivatives with respect to ζ ,

$$\begin{aligned} \frac{dE_\Theta}{d\zeta} &= \frac{d\mathcal{L}_\Theta}{d\zeta} = \frac{\partial \mathcal{L}_\Theta}{\partial \hat{H}} \frac{d\hat{H}}{d\zeta} + \underbrace{\frac{\partial \mathcal{L}_\Theta}{\partial \theta_i}}_0 \frac{\partial \theta_i}{\partial \zeta} + \underbrace{\frac{\partial \mathcal{L}_\Theta}{\partial \tilde{\theta}_i}}_0 \frac{\partial \tilde{\theta}_i}{\partial \zeta} \\ &= \boxed{\frac{\partial \mathcal{L}_\Theta}{\partial \hat{H}} \frac{d\hat{H}}{d\zeta}} \end{aligned} \quad (5)$$

Though note that,

$$\frac{\partial \mathcal{L}_\Theta}{\partial \hat{H}} = \frac{\partial E_\Theta}{\partial \hat{H}} + \sum_i \tilde{\theta}_i \frac{\partial f_i}{\partial \hat{H}} \quad (6)$$

The last term contains the additional “response” contributions to the gradient - these are generally computationally expedient to build once the Lagrange multipliers $\{\tilde{\theta}_i\}$ are determined. Also note that the second term in the final chain rule expression is written $d_\zeta \hat{H}$ rather than $\partial_\zeta \hat{H}$ - this is because \hat{H} might itself have implicit parameters in ζ , for which a separate set response equations will have to be solved and corresponding response contributions accounted for. This will occur in a key place in the present manuscript - one set of Lagrangians will be built, fully variationally optimized, and then differentiated in the quantum part of the MC-VQE algorithm to determine the quantum gradient in the AIEM monomer basis. Subsequently, a second set of (now fully classical) Lagrangians will be built, fully variationally optimized, and then differentiated to determine the contributions of the classical AIEM matrix elements to the total gradient. This nesting provides a natural separation between the quantum and classical parts of the MC-VQE+AIEM gradient algorithm, and should prove to be a general feature

of hybrid quantum/classical analytical derivative methods in other Hamiltonian representations.

As a final note, we point out that, by convention, the particular derivative quantity,

$$\hat{\Gamma} \equiv \frac{dE_\Theta}{d\hat{H}} = \frac{\partial \mathcal{L}_\Theta}{\partial \hat{H}} \quad (7)$$

is referred to as the “relaxed density matrix,” while the corresponding derivative quantity,

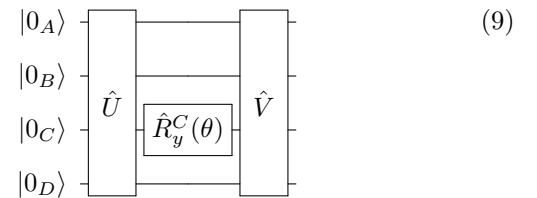
$$\hat{\Gamma}^0 \equiv \frac{\partial E_\Theta}{\partial \hat{H}} \quad (8)$$

is referred to as the “unrelaxed density matrix.”

B. Circuit Gradients and Hessians

A key technical ingredient in the hybrid quantum/classical analytical derivative methodology developed below is an efficient and robust approach to compute the analytical derivatives of quantum circuit observable expectation values with respect to perturbations in the gate angle parameters of the quantum circuit. Particularly, finite difference approaches are entirely unacceptable due to extreme precision requirements in the involved observables, which would require intractable statistical convergence and noise requirements. Here, we exploit known tomography formulae for the dependency of quantum circuit observable expectation values on a handful of active gate angles to develop formulae for the gradient and Hessian that require determination of the observable expectation value on a stencil of widely-spaced gate angles, with similar statistical convergence requirements as required for the original observable expectation values.

Consider a quantum circuit starting with the reference state $|\vec{0}\rangle$, proceeding through an arbitrary unitary \hat{U} , thence through a parametrized \hat{R}_y gate with parameter θ acting on qubit C (an arbitrary qubit index), e.g., $\hat{R}_y^C(\theta) \equiv e^{-i\theta \hat{Y}_C}$, and finally through an arbitrary unitary \hat{V} . I.e., sketched in circuit form,



The expectation value of an observable operator \hat{O} is,

$$O(\theta) = \langle \hat{O} \rangle = \langle \vec{0} | \hat{U}^\dagger \hat{R}_y^C(\theta) \hat{V}^\dagger \hat{O} \hat{V} \hat{R}_y^C(\theta) \hat{U} | \vec{0} \rangle \quad (10)$$

It can be shown that this expectation value always exactly follows a sinusoidal dependence,

$$O(\theta - \theta_0) = A + B \cos(2(\theta - \theta_0)) + C \sin(2(\theta - \theta_0)) \quad (11)$$

where θ_0 is the current setting of the gate angle. The three circuit-specific tomography coefficients A , B , and C can be determined by sampling O at any three angles. Particularly, sampling at $O^0 \equiv O(\theta_0)$ and $O^\pm \equiv O(\theta_0 \pm \pi/4)$ yields,

$$C = (O^+ - O^-)/2 \quad (12)$$

$$A = (O^+ + O^-)/2 \quad (13)$$

$$B = O^0 - (O^+ + O^-)/2 \quad (14)$$

With the tomography coefficients resolved, the first derivative is now analytical,

$$\begin{aligned} \frac{\partial O(\theta)}{\partial \theta} &= \langle \vec{0} | \hat{U}^\dagger \hat{R}_y^{C\dagger}(\theta + \pi/4) \hat{V}^\dagger \hat{O} \hat{V} \hat{R}_y^C(\theta + \pi/4) \hat{U} | \vec{0} \rangle \\ &\quad - \langle \vec{0} | \hat{U}^\dagger \hat{R}_y^{C\dagger}(\theta - \pi/4) \hat{V}^\dagger \hat{O} \hat{V} \hat{R}_y^C(\theta - \pi/4) \hat{U} | \vec{0} \rangle \\ &= \boxed{O(\theta + \pi/4) - O(\theta - \pi/4)} \end{aligned} \quad (15)$$

This is remarkable when we consider the symmetric finite-difference formula with stepsize h ,

$$\begin{aligned} \frac{\partial O(\theta)}{\partial \theta} &= O(\theta + \pi/4) - O(\theta - \pi/4) \\ &\approx \frac{1}{2h} [O(\theta + h) - O(\theta - h)] \end{aligned} \quad (16)$$

This can easily be extended to higher-order derivatives, by inspection,

$$\begin{aligned} \frac{\partial^2 O(\theta)}{\partial \theta^2} &= O(\theta + \pi/2) - 2O(\theta) + O(\theta - \pi/2) \\ &\approx \frac{1}{4h^2} [O(\theta + 2h) - 2O(\theta) + O(\theta - 2h)] \end{aligned} \quad (17)$$

and,

$$\begin{aligned} \frac{\partial^2 O(\theta, \theta')}{\partial \theta \partial \theta'} &= O(\theta + \pi/4, \theta' + \pi/4) - O(\theta + \pi/4, \theta' - \pi/4) \\ &\quad - O(\theta - \pi/4, \theta' + \pi/4) + O(\theta - \pi/4, \theta' - \pi/4) \\ &\approx \frac{1}{4h^2} [O(\theta + h, \theta' + h) - O(\theta + h, \theta' - h) \\ &\quad - O(\theta - h, \theta' + h) + O(\theta - h, \theta' - h)] \end{aligned} \quad (18)$$

A key observation is that the coefficients of the observables in tomography-based formulae for the gradients and Hessians are of order unity, in contrast to the $1/h$ or $1/h^2$

coefficients of the finite-difference formulae. This implies that the tomography-based formulae do not experience subtractive cancellation, and may be evaluated with similar statistical precision as the underlying observables to obtain similar absolute accuracy in the derivative quantities.

Note that many other three-point quadratures can be used to analytically/exactly resolve the tomography coefficients of Equation 11 and it's multi- \hat{R}_y -gate counterpart, and to compute the corresponding derivatives. For instance, the three-point Fourier grid with collocation points $\{-\pi/3, 0, +\pi/3\}$ can be used, and only the minutia of the quadrature collocation-to-tomography coefficient transformation changes.

III. EXPLICIT MC-VQE+AIEM ENERGY AND GRADIENT RECIPE

In this section, we carefully define and then differentiate the MC-VQE+AIEM adiabatic state energies. The flow of this section roughly follows reverse accumulation automatic differentiation, with a Lagrangian approach used for implicit portions of the derivatives.

1. Indices

The following index classes are used in this work,

- A - Monomer.
- I - Contracted reference state (CRS) configuration, e.g., configuration interaction singles (CIS) configuration.
- Ξ - CRS eigenstate.
- Θ - MC-VQE eigenstate.
- M - CIS quantum circuit angle.
- g - VQE entangler quantum circuit angle.
- ζ - Nuclear gradient perturbation.

Primes are used to distinguish repeated indices.

A. Classical AIEM Energy Stage

1. Monomer Properties

To begin, for an *ab initio* exciton model (AIEM) with N neutral monomers, each with two relevant electronic states, and with restricted two-body interactions computed in the dipole-dipole approximation, compute the following quantities at the current nuclear positions $\{\vec{r}_\zeta\}$.

- ϵ_{H}^A : The energy of the singlet ground (hole) state of the monomer.

- ϵ_{P}^A : The energy of the first singlet excited (particle) state of the monomer.
- $\vec{\mu}_{\text{H}}^A$: The total dipole moment of the hole state of the monomer.
- $\vec{\mu}_{\text{P}}^A$: the total dipole moment of the particle state of the monomer.
- $\vec{\mu}_{\text{T}}^A$: the transition dipole moment between the hole and particle states.
- \vec{r}_0^A : The geometric centroid of the monomer, e.g., the center of mass of the nuclei, $\vec{r}_0^A \equiv \sum_{\zeta} m_{\zeta} \vec{r}_{\zeta} / \sum_{\zeta'} m_{\zeta'}$, where \vec{r}_{ζ} is the Cartesian coordinates of atom ζ and m_{ζ} is the mass of atom ζ .

These quantities can all be computed efficiently by classical electronic structure methods that scale only with the monomer size, and which are independent of the total size of the system N . For instance, today we will use ground-state Kohn-Sham density function theory (KS-DFT) to compute the ground-state monomer properties ϵ_{H}^A and $\vec{\mu}_{\text{H}}^A$, and the Tamm-Dancoff approximation for time-dependent density functional theory (TDA-TD-DFT) TDA-TD-DFT to compute the excited state and transition properties ϵ_{P}^A , $\vec{\mu}_{\text{P}}^A$, and $\vec{\mu}_{\text{T}}^A$ (excited state and transition dipole moments computed in the unrelaxed expectation value formulation), though many other electronic structure methods could also be used.

It may be convenient to also compute the analytical nuclear gradients of all of these monomer properties at this stage in the computation: $\epsilon_{\text{H}}^{A,\zeta}$, $\epsilon_{\text{P}}^{A,\zeta}$, $\vec{\mu}_{\text{H}}^{A,\zeta}$, $\vec{\mu}_{\text{P}}^{A,\zeta}$, $\vec{\mu}_{\text{T}}^{A,\zeta}$, and $\vec{r}_0^{A,\zeta}$ will all be required at the very end of this procedure. Here, e.g., $\epsilon_{\text{H}}^{A,\zeta} \equiv d_{\vec{r}_{\zeta}} \epsilon_{\text{H}}^A$. The computation of these analytical derivatives of classical monomer properties often requires a Lagrangian formalism and the solution of classical response equations, e.g., coupled-perturbed Kohn-Sham (CP-KS) equations must be solved in the computation of $\epsilon_{\text{P}}^{A,\zeta}$, $\vec{\mu}_{\text{H}}^{A,\zeta}$, $\vec{\mu}_{\text{P}}^{A,\zeta}$, and $\vec{\mu}_{\text{T}}^{A,\zeta}$. Note that these response equations may be solved separately from the quantum response equations that will appear later in the procedure. Alternatively, if one wishes to follow the spirit of the Lagrangian formalism to its zenith, these monomer derivative property computations can be deferred to the very end of the procedure, in which case they will appear as chain rule terms contracted against density matrix quantities from the quantum portion of the algorithm. This formulation can provide enhanced screening if some density matrix elements are small, and can also reduce the number of classical response equations that must be explicitly computed. E.g., the hole dipole chain-rule contribution is $E_{\Theta}^{A,\zeta} \leftarrow \vec{\eta}_{\text{H}}^{A,\Theta} \vec{\mu}_{\text{H}}^{A,\zeta}$, which can be computed with a single CP-KS response if the hole dipole density matrix $\vec{\eta}_{\text{H},\Theta}^A$ is available, vs three separate CP-KS response contributions to compute the Cartesian hole dipole derivatives $\vec{\mu}_{\text{H}}^{A,\zeta}$ beforehand.

2. Dimer Interaction Matrix Elements

In the present work, electrostatic interactions between monomers are computed in the dipole-dipole approximation,

$$v^{AA'} = \frac{\vec{\mu}_A \cdot \vec{\mu}_{A'}}{r_{AA'}^3} - 3 \frac{(\vec{\mu}_A \cdot \vec{r}_{AA'}) (\vec{\mu}_{A'} \cdot \vec{r}_{AA'})}{r_{AA'}^5} \quad (19)$$

Here $\vec{r}_{AA'} \equiv \vec{r}_0^{A'} - \vec{r}_0^A$, and $r_{AA'} = \sqrt{|\vec{r}_{AA'}|^2}$. The dipole moments run over the types of H, T, and P for monomers A and A' , leading to $9 \times$ possible two-body coupling matrix elements for a given A, A' pair: $v_{\text{HH}}^{AA'}$, $v_{\text{HT}}^{AA'}$, $v_{\text{HP}}^{AA'}$, $v_{\text{TH}}^{AA'}$, $v_{\text{TT}}^{AA'}$, $v_{\text{TP}}^{AA'}$, $v_{\text{PH}}^{AA'}$, $v_{\text{PT}}^{AA'}$, and $v_{\text{PP}}^{AA'}$. Note the symmetries, $v_{\text{HH}}^{AA'} = v_{\text{HH}}^{A'A}$, $v_{\text{TT}}^{AA'} = v_{\text{TT}}^{A'A}$, $v_{\text{PP}}^{AA'} = v_{\text{PP}}^{A'A}$, $v_{\text{HT}}^{AA'} = v_{\text{TH}}^{A'A}$, $v_{\text{HP}}^{AA'} = v_{\text{PH}}^{A'A}$, and $v_{\text{TP}}^{AA'} = v_{\text{PT}}^{A'A}$. Due to the $r_{AA'}^{-3}$ decay of these matrix elements, distant A, A' pairs may often be eliminated with insignificant errors (e.g., today we assert a nearest-neighbor-only coupling model, for simplicity). We denote the set of significant A, A' pairs included in the AIEM by the notation $\langle A, A' \rangle$ (including both $A > A'$ and $A < A'$). Note that $A = A'$ pairs are never included - these are already accounted for in the one-body matrix elements ϵ_{H}^A and ϵ_{P}^A .

Also note that it is entirely possible to go beyond the dipole-dipole approximation for these dimer interaction matrix elements: in prior work we have also used fully *ab initio* matrix elements involving the electrostatic interactions between state or transition densities to account for higher-order multipole contributions and charge penetration terms. Such matrix elements could easily be used within MC-VQE+AIEM energies and derivatives, though the full Lagrangian formalism discussed above would be useful to avoid having to explicitly form the derivatives of the two-body matrix elements $v^{AA',\zeta}$.

3. Monomer-Basis AIEM Hamiltonian

In the monomer basis, the AIEM Hamiltonian is succinctly written as,

$$\begin{aligned} \hat{H} &\equiv \hat{H}^{(1)} + \hat{H}^{(2)} \quad (20) \\ &= \sum_A \sum_{p,q \in [0,1]} (p_A | \hat{h} | q_A) |p_A\rangle \langle q_A| \\ &+ \frac{1}{2} \sum_{\langle A, A' \rangle} \sum_{p,q,r,s \in [0,1]} (p_A q_A | \hat{h} | r_{A'} s_{A'}) |p_A\rangle \langle q_A| \otimes |r_{A'}\rangle \langle s_{A'}| \end{aligned}$$

Where now $|0_A\rangle$ refers to the monomer ground state (hole), $|1_A\rangle$ refers to the monomer excited state (particle), and in chemist's notation $|00\rangle$ refers to H (hole), $|11\rangle$ refers to P (particle), and $|01\rangle$ or $|10\rangle$ refers to T (transition). Note that the correspondence of the matrix elements is,

$$(0_A | \hat{h} | 0_A) = \epsilon_{\text{H}}^A \quad (21)$$

$$(1_A|\hat{h}|1_A) = \epsilon_P^A \quad (22)$$

$$(0_A|\hat{h}|1_A) = (1_A|\hat{h}|0_A) = 0 \quad (23)$$

$$(0_A 0_A|\hat{v}|0_{A'} 0_{A'}) = v_{\text{HH}}^{AA'} \quad (24)$$

$$(0_A 0_A|\hat{v}|1_{A'} 1_{A'}) = v_{\text{HP}}^{AA'} \quad (25)$$

$$(1_A 1_A|\hat{v}|0_{A'} 0_{A'}) = v_{\text{PH}}^{AA'} \quad (26)$$

$$(1_A 1_A|\hat{v}|1_{A'} 1_{A'}) = v_{\text{PP}}^{AA'} \quad (27)$$

$$(0_A 0_A|\hat{v}|0_{A'} 1_{A'}) = (0_A 0_A|\hat{v}|1_{A'} 0_{A'}) = v_{\text{HT}}^{AA'} \quad (28)$$

$$(0_A 1_A|\hat{v}|0_{A'} 0_{A'}) = (1_A 0_A|\hat{v}|0_{A'} 0_{A'}) = v_{\text{TH}}^{AA'} \quad (29)$$

$$(1_A 1_A|\hat{v}|0_{A'} 1_{A'}) = (1_A 1_A|\hat{v}|1_{A'} 0_{A'}) = v_{\text{PT}}^{AA'} \quad (30)$$

$$(0_A 1_A|\hat{v}|1_{A'} 1_{A'}) = (1_A 0_A|\hat{v}|1_{A'} 1_{A'}) = v_{\text{TP}}^{AA'} \quad (31)$$

$$(0_A 1_A|\hat{v}|0_{A'} 1_{A'}) = (0_A 1_A|\hat{v}|1_{A'} 0_{A'}) \quad (32)$$

$$= (1_A 0_A|\hat{v}|0_{A'} 1_{A'}) = (1_A 0_A|\hat{v}|1_{A'} 0_{A'}) = v_{\text{TT}}^{AA'}$$

In practice, the monomer-basis representation of the AIEM Hamiltonian is only used for a formal definition: in computational practice, we transition immediately from the definition of the matrix elements in the previous section to the Pauli-basis representation of the AIEM Hamiltonian in the following section.

4. Pauli-Basis AIEM Hamiltonian

After some straightforward algebra, the AIEM Hamiltonian can be succinctly re-written in terms of Pauli operators,

$$\begin{aligned} \hat{H} &\equiv \mathcal{E} + \mathcal{H}^{(1)} + \mathcal{H}^{(2)} = \mathcal{E}\hat{I} + \sum_A \mathcal{Z}_A \hat{Z}_A + \mathcal{X}_A \hat{X}_A \\ &+ \frac{1}{2} \sum_{\langle A, A' \rangle} \mathcal{X} \mathcal{X}_{AA'} \hat{X}_A \otimes \hat{X}_{A'} + \mathcal{X} \mathcal{Z}_{AA'} \hat{X}_A \otimes \hat{Z}_{A'} \\ &+ \mathcal{Z} \mathcal{X}_{AA'} \hat{Z}_A \otimes \hat{X}_{A'} + \mathcal{Z} \mathcal{Z}_{AA'} \hat{Z}_A \otimes \hat{Z}_{A'} \quad (33) \end{aligned}$$

The matrix elements are,

$$\mathcal{E} = \sum_A (\epsilon_{\text{H}}^A + \epsilon_{\text{P}}^A)/2 + \frac{1}{2} \sum_{\langle A, A' \rangle} (v_{\text{HH}}^{AA'} + v_{\text{HP}}^{AA'} + v_{\text{PH}}^{AA'} + v_{\text{PP}}^{AA'})/4$$

$$\equiv \sum_A \epsilon_{\text{S}}^A + \frac{1}{2} \sum_{\langle A, A' \rangle} v_{\text{SS}}^{AA'} \quad (34)$$

$$\begin{aligned} \mathcal{X}_A &= \underbrace{\epsilon_{\text{T}}^A}_0 + \frac{1}{2} \sum_{A'} (v_{\text{TH}}^{AA'} + v_{\text{TP}}^{AA'})/2 + (v_{\text{HT}}^{A'A} + v_{\text{PT}}^{A'A})/2 \\ &\equiv \underbrace{\epsilon_{\text{T}}^A}_0 + \frac{1}{2} \sum_{A'} v_{\text{TS}}^{AA'} + v_{\text{ST}}^{A'A} \quad (35) \end{aligned}$$

$$\mathcal{Z}_A = (\epsilon_{\text{H}}^A - \epsilon_{\text{P}}^A)/2$$

$$\begin{aligned} &+ \frac{1}{2} \sum_{A'} (v_{\text{HH}}^{AA'} + v_{\text{HP}}^{AA'} - v_{\text{PH}}^{AA'} - v_{\text{PP}}^{AA'})/4 \\ &+ (v_{\text{HH}}^{A'A} + v_{\text{PH}}^{A'A} - v_{\text{HP}}^{A'A} - v_{\text{PP}}^{A'A})/4 \\ &\equiv \epsilon_{\text{D}}^A + \frac{1}{2} \sum_{A'} v_{\text{SD}}^{AA'} + v_{\text{DS}}^{A'A} \quad (36) \end{aligned}$$

$$\mathcal{X} \mathcal{X}_{AA'} = v_{\text{TT}}^{AA'} \quad (37)$$

$$\mathcal{X} \mathcal{Z}_{AA'} = (v_{\text{TH}}^{AA'} - v_{\text{TP}}^{AA'})/2 \equiv v_{\text{TD}}^{AA'} \quad (38)$$

$$\mathcal{Z} \mathcal{X}_{AA'} = (v_{\text{HT}}^{AA'} - v_{\text{PT}}^{AA'})/2 \equiv v_{\text{DT}}^{AA'} \quad (39)$$

$$\mathcal{Z} \mathcal{Z}_{AA'} = (v_{\text{HH}}^{AA'} - v_{\text{HP}}^{AA'} - v_{\text{PH}}^{AA'} + v_{\text{PP}}^{AA'})/4 \equiv v_{\text{DD}}^{AA'} \quad (40)$$

Here the new letters are S (sum) and D (difference). \hat{I} operators correspond to S, \hat{X} operators correspond to T, and \hat{Z} operators correspond to D.

B. Quantum MC-VQE Energy Stage

1. Formal Definition: MC-VQE Eigenstates

MC-VQE approximates the exact diagonalization of the Pauli Hamiltonian \hat{H} by producing a number N_{Θ} of MC-VQE approximate eigenstates $|\Psi_{\Theta}\rangle$.

$$|\Psi_{\Theta}\rangle \equiv \hat{U}(\theta_g) \sum_{\Xi} |\Phi_{\Xi}\rangle V_{\Xi\Theta} \quad (41)$$

$$= \hat{U}(\theta_g) \sum_I \sum_{\Xi} |I\rangle C_{I\Xi} V_{\Xi\Theta} \quad (42)$$

$$= \hat{U}(\theta_g) \sum_I |I\rangle \Gamma_{I\Theta} \quad (43)$$

$$= \hat{U}(\theta_g)|\Gamma_\Theta\rangle \quad (44)$$

The MC-VQE eigenstates are orthonormal,

$$\langle\Psi_\Theta|\Psi_{\Theta'}\rangle = \delta_{\Theta\Theta'} \quad (45)$$

and within the MC-VQE contracted, entangled subspace, the Hamiltonian is diagonal,

$$\langle\Psi_\Theta|\hat{H}|\Psi_{\Theta'}\rangle = E_\Theta\delta_{\Theta\Theta'} \quad (46)$$

Specific quantities are defined below.

2. Configuration Interaction Singles Contracted Reference States

To begin, we classically determine a number $N_\Xi = N_\Theta$ of “contracted reference states” (CRS), $\{|\Phi_\Xi\rangle\}$, by solving a polynomial-scaling electronic structure problem to “sketch out” the shapes of the desired electronic states. One particularly appealing choice for the contracted reference states is the set of eigenstates of a restricted configuration interaction method, such as configuration interaction singles (CIS),

Form the configuration interaction singles (CIS) Hamiltonian. This matrix is indexed by a restricted set of configurations $\{|I\rangle\} \equiv \{|0\rangle\} + \{|A\rangle\}$ consisting of the reference configuration $|0\rangle \equiv |00\dots 0\rangle$, followed by the N singly-excited configurations $\{|A\rangle\}$ including $|10\dots 0\rangle$, $|01\dots 0\rangle$, and finally $|00\dots 1\rangle$ ($N+1$ configurations total). The CIS Hamiltonian has the block form,

$$\hat{H}_{\text{CIS}} \equiv \begin{bmatrix} H_{00} & H_{0A'} \\ H_{A0} & H_{AA'} \end{bmatrix} \quad (47)$$

The reference-reference block is,

$$H_{00} = \langle 0|\hat{H}|0\rangle = \mathcal{E} + \sum_A \mathcal{Z}_A + \frac{1}{2} \sum_{\langle A,A'\rangle} \mathcal{Z}\mathcal{Z}_{AA'} \equiv E_{\text{ref}} \quad (48)$$

The diagonal singles-singles block is,

$$H_{AA} = \langle A|\hat{H}|A\rangle = E_{\text{ref}} - 2\mathcal{Z}_A - \sum_{A'} [\mathcal{Z}\mathcal{Z}_{AA'} + \mathcal{Z}\mathcal{Z}_{A'A}] \quad (49)$$

The reference-singles block is,

$$H_{0A} = H_{A0} = \langle 0|\hat{H}|A\rangle = \mathcal{X}_A + \frac{1}{2} \sum_{A'} [\mathcal{X}\mathcal{Z}_{AA'} + \mathcal{Z}\mathcal{X}_{A'A}] \quad (50)$$

The off-diagonal singles-singles block is,

$$H_{A\neq A'} = \langle A|\hat{H}|A'\rangle|_{A\neq A'} = \mathcal{X}\mathcal{X}_{AA'} \quad (51)$$

Now, classically diagonalize the CIS Hamiltonian to obtain the CIS contracted reference states (CRS),

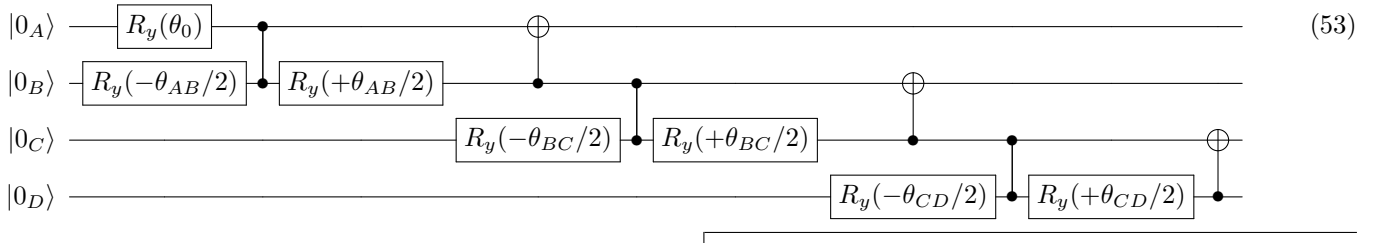
$$|\Phi_\Xi\rangle \equiv \sum_I |I\rangle C_{I\Xi} : \sum_J H_{IJ} C_{J\Xi} = C_{I\Xi} E_\Xi^{\text{CIS}}, \quad (52) \\ \sum_I C_{I\Xi} C_{I\Xi'} = \delta_{\Xi\Xi'}$$

Note that we often focus on $N_\Theta = N_\Xi \leq N_I$ - from this point forward, it is assumed that any Θ or Ξ index only runs up to N_Θ .

Note that other choices of contracted reference states would lead to different forms/results for the MC-VQE eigenstates and different response contributions in analytical derivatives, but the manipulations would be similar. One particularly interesting alternative example is the use of single configurations (e.g., “determinants”) or *a priori* known combinations of several configurations (e.g., “configuration state functions”) - here, no implicit equations are solved to determine the contracted reference states, and so no response terms would appear in the corresponding analytical derivatives.

3. Technical Detail: CIS State Preparation Circuit

A quantum circuit to prepare the CIS state $|\Phi\rangle \equiv \sum_I |I\rangle C_I \equiv \hat{U}_{\text{CIS}}|0\rangle$ is sketched for $N=4$,



The $R_y(\theta_0)$ gate controls the amplitude of the reference

ket $|00\dots\rangle$, while the composite two-body gates between

each pair of wires control the amplitudes of each singly-excited ket $|10\dots\rangle$, $|01\dots\rangle$, etc. Specifically, the com-

posite two-body gate is,

$$\begin{array}{c} \text{---} \\ \text{---} \end{array} \begin{array}{c} \boxed{R_y(-\theta/2)} \\ \boxed{R_y(+\theta/2)} \end{array} \text{---} \text{---} \text{---} \oplus \text{---} = \begin{bmatrix} 1 & \\ & +s(\theta) & -c(\theta) \\ & +c(\theta) & +s(\theta) \\ & & & 1 \end{bmatrix} \quad (54)$$

The action of this composite two-body gate on a statevector of the form $\mu|00\rangle + \mu'|10\rangle$ yields a statevector of the form $\mu|00\rangle + \alpha|10\rangle + \beta|01\rangle$, where $\alpha = \mu' \cos(\theta)$ and $\beta = \mu' \sin(\theta)$.

$$\begin{bmatrix} 1 & & & \\ & +s(\theta) & -c(\theta) & \\ & +c(\theta) & +s(\theta) & \\ & & & 1 \end{bmatrix} \begin{bmatrix} \mu \\ 0 \\ \mu' \\ 0 \end{bmatrix} = \begin{bmatrix} \mu \\ \mu' s(\theta) \\ \mu' c(\theta) \\ 0 \end{bmatrix} \quad (55)$$

E.g., this gate transfers single excitation from qubit A to qubit B . We note that there are many possibly choices for the composite two-body gates and the overall CIS state preparation circuit; the definition used here is merely pragmatic. Overall, our selected CIS state preparation circuit requires a linear number of gates and, as written, requires linear depth with only linear nearest-neighbor qubit connectivity - a drastic simplification over our previous efforts which used a quadratic sequence of CNOT gates. It is worth noting that it appears that this state-preparation circuit can be extended to use logarithmic depth at the cost of higher two-qubit connectivity and modified definitions of the gate angles, e.g., by moving from a linear control sequence to a binary-tree control sequence.

By inspection, it is straightforward to classically determine the CIS circuit gate angles from the CIS wavefunction amplitudes,

$$\theta_0 = \cos^{-1} \left(C_0 / \sqrt{C_0^2 + C_A^2 + \dots + C_N^2} \right) \quad (56)$$

$$\theta_{AB} = \cos^{-1} \left(C_A / \sqrt{C_A^2 + C_B^2 + \dots + C_N^2} \right) \quad (57)$$

$$\vdots \quad (58)$$

$$\theta_{MN} = \text{sign}(C_N) \cos^{-1} \left(C_M / \sqrt{C_M^2 + C_N^2} \right) \quad (59)$$

Note that the raw value of the last CIS coefficient C_N is not used inside of the arccos formula set, so an additional phase factor appears in the last angle to preserve the total information content of the CIS coefficient vector.

A succinct classical function to return the N CIS circuit angles $\{\theta_M\}$ for an arbitrary normalized CIS state with $N + 1$ coefficients $\{C_I\}$ is,

$$\theta_M[C_I] \equiv P_M \cos^{-1} \left(\frac{C_M}{\sqrt{\sum_{L=M}^N C_L^2}} \right), \quad M \in [0, N - 1] \quad (60)$$

$$P_M \equiv \begin{cases} \text{sign}(C_N) & M = N - 1 \\ 1 & \text{else} \end{cases} \quad (61)$$

We will need this function in several places, with a number of different choices for the $N + 1$ input CIS coefficients $\{C_I\}$. Another function that will prove to be extremely useful is the contraction of an arbitrary N -dimensional vector d_M with the Jacobian $\partial\theta_M[C_I]/\partial C_I$,

$$\begin{aligned} \frac{dO}{dC_I}[C_I, d_M] &\equiv \sum_M \underbrace{\frac{\partial O}{\partial \theta_M[C_I]}}_{d_M} \frac{\partial \theta_M[C_I]}{\partial C_I} \quad (62) \\ &= \sum_M d_M P_M \left[-\frac{\delta_{MI}}{\sqrt{\sum_{L=M+1}^N C_L^2}} \right. \\ &\quad \left. + \frac{C_M C_I \delta_{I \geq M}}{\sqrt{\sum_{L=M+1}^N C_L^2} \left(\sum_{K=M}^N C_K^2 \right)} \right] \end{aligned}$$

4. CIS Circuit Angles

Using the recipe from the previous section, compute the N CIS circuit angles from the $N + 1$ CIS coefficients, for each state Ξ :

$$\theta_M[C_I \Xi] \quad (63)$$

5. State-Averaged VQE

A key step in MC-VQE is the use of a state-averaged VQE entangler operator $\hat{U}_{\text{VQE}}(\theta_g)$ to maximally decouple the contracted reference states $\{|\Phi_\Xi\rangle\}$ from the rest of

the Hilbert space, i.e., using the VQE entangler operator to maximally block-diagonalize the Hamiltonian. This VQE entangler operator acts over the full qubit Hilbert space (tractable because of the use of a quantum computer), and is specified by a polynomial number of nonlinear parameters $\{\theta_g\}$. The maximal decoupling condition is equivalent (in the 2-norm sense) to minimizing the state-averaged energy,

$$\hat{U}_{\text{VQE}}(\theta_g) = \underset{\hat{U}_{\text{VQE}}(\theta_g)}{\text{argmin}} [\bar{E}] \quad (64)$$

which is defined as,

$$\bar{E} \equiv \frac{1}{N_\Theta} \sum_{\Theta} E_\Theta \equiv \frac{1}{N_\Theta} \sum_{\Theta} \langle \Psi_\Theta | \hat{H} | \Psi_\Theta \rangle \quad (65)$$

$$= \frac{1}{N_\Theta} \sum_{\Xi} \langle \Phi_\Xi | \hat{U}_{\text{VQE}}^\dagger \hat{H} \hat{U}_{\text{VQE}} | \Phi_\Xi \rangle \quad (66)$$

where \hat{H} is the Hamiltonian operator in the qubit Hilbert space. The MC-VQE state energy is defined as,

$$E_\Theta \equiv \langle \Psi_\Theta | \hat{H} | \Psi_\Theta \rangle \quad (67)$$

The weak form of the state-averaged variational condition is the zero-gradient condition,

$$\frac{\partial \bar{E}}{\partial \theta_g} = 0 \quad (68)$$

Let us consider a key set of Pauli density matrices, which are defined as a function for an arbitrary set of CIS state preparation angles $\{\theta_M\}$ and an arbitrary set of VQE \hat{R}_y gate parameter angles $\{\theta_g\}$, e.g.,

$$\lambda_{\mathcal{Z}_A}[\theta_g, \theta_M] \equiv \quad (69)$$

$$\langle 0 | \hat{U}_{\text{CIS}}^\dagger[\theta_M] \hat{U}_{\text{VQE}}^\dagger[\theta_g] \hat{Z}_A \hat{U}_{\text{VQE}}[\theta_g] \hat{U}_{\text{CIS}}[\theta_M] | 0 \rangle$$

or,

$$\Lambda_{\mathcal{Z}\mathcal{Z}_{AA'}}[\theta_g, \theta_M] \equiv \quad (70)$$

$$\langle 0 | \hat{U}_{\text{CIS}}^\dagger[\theta_M] \hat{U}_{\text{VQE}}^\dagger[\theta_g] \hat{Z}_A \otimes \hat{Z}_{A'} \hat{U}_{\text{VQE}}[\theta_g] \hat{U}_{\text{CIS}}[\theta_M] | 0 \rangle$$

These can be evaluated by statistically-converged tomography measurements of quantum circuits passing through a CIS-state preparation stage \hat{U}_{CIS} and a VQE stage \hat{U}_{VQE} with the specified parameters. Many of the measurements correspond to commuting operators in disjoint sets of qubits, and can be performed in parallel. Measurements in the \hat{X} basis can be easily made by postpending the circuit with a Hadamard gate(s) in the appropriate position(s). Note that we will require the one-body Pauli density matrices for all one-body elements \mathcal{Z}_A and \mathcal{X}_A , and for all two-body elements $\mathcal{X}\mathcal{X}_{AA'}$, $\mathcal{X}\mathcal{Z}_{AA'}$, $\mathcal{Z}\mathcal{X}_{AA'}$, $\mathcal{Z}\mathcal{Z}_{AA'}$, for all A, A' pairs in $\langle A, A' \rangle$.

The energy of a VQE-entangled CIS contracted reference state is, with appropriate parameters,

$$\varepsilon[\{\theta_g, \theta_M\}] \equiv \mathcal{E} + \sum_A \lambda_{\mathcal{Z}_A} \mathcal{Z}_A + \lambda_{\mathcal{X}_A} \mathcal{X}_A \quad (71)$$

$$+ \frac{1}{2} \sum_{\langle A, A' \rangle} \Lambda_{\mathcal{X}\mathcal{X}_{AA'}} \mathcal{X}\mathcal{X}_{AA'} + \Lambda_{\mathcal{X}\mathcal{Z}_{AA'}} \mathcal{X}\mathcal{Z}_{AA'}$$

$$+ \Lambda_{\mathcal{Z}\mathcal{X}_{AA'}} \mathcal{Z}\mathcal{X}_{AA'} + \Lambda_{\mathcal{Z}\mathcal{Z}_{AA'}} \mathcal{Z}\mathcal{Z}_{AA'}$$

This energy can be computed classically after the Pauli density matrices have been evaluated. Note that only the Pauli density matrices $\{\lambda\}$ and $\{\Lambda\}$ depend on the CIS or VQE parameters $\{\theta_M\}$ or $\{\theta_g\}$.

A useful specialization to VQE-entangled CIS contracted reference states is,

$$\lambda_{\mathcal{Z}_A}^\Xi[\theta_g] \equiv \lambda_{\mathcal{Z}_A}[\theta_g, \theta_M[C_{I\Xi}]] \quad (72)$$

and the corresponding energy is,

$$\varepsilon^\Xi[\theta_g] \equiv H_{\Xi\Xi} = \varepsilon[\theta_g, \theta_M[C_{I\Xi}]] \quad (73)$$

A further specialization to state-averaged VQE-entangled CIS contracted reference states is,

$$\bar{\lambda}_{\mathcal{Z}_A}[\theta_g] \equiv \frac{1}{N_\Theta} \sum_{\Xi} \lambda_{\mathcal{Z}_A}^\Xi[\theta_g] \quad (74)$$

and the corresponding state-averaged MC-VQE energy is,

$$\bar{E}[\theta_g] \equiv \frac{1}{N_\Theta} \sum_{\Xi} \varepsilon^\Xi[\theta_g] \quad (75)$$

The goal of the hybrid quantum/classical MC-VQE optimization procedure is to find the set of VQE parameters $\{\theta_g^*\}$ that minimize the state-averaged VQE energy,

$$\{\theta_g^*\} \equiv \underset{\{\theta_g\}}{\text{argmin}} (\bar{E}[\theta_g]) \quad (76)$$

To aid in the optimization, it can be useful to have the gradient of the state-averaged VQE energy for a given set of VQE parameters,

$$\frac{\partial \bar{E}[\theta_{g'}]}{\partial \theta_g} \quad (77)$$

E.g., the weak form of the state-averaged VQE functional is the stationary condition,

$$\frac{\partial \bar{E}[\theta_{g'}^*]}{\partial \theta_g} = 0 \quad \forall g \quad (78)$$

Moreover (subject to noise constraints), the state-averaged VQE energy optimization procedure can use gradient-based optimization algorithms such as L-BFGS

to enhance the convergence of the MC-VQE energy functional.

The gradients with respect to the VQE parameters are,

$$\frac{\partial \bar{E}[\theta_{g'}]}{\partial \theta_g} = \frac{1}{N_{\Theta}} \sum_{\Xi} \frac{\partial \varepsilon^{\Xi}[\theta_{g'}]}{\partial \theta_g} \quad (79)$$

and,

$$\frac{\partial \varepsilon^{\Xi}[\theta_{g'}]}{\partial \theta_g} \equiv \sum_A (\partial_{\theta_g} \lambda_{\mathcal{Z}_A}^{\Xi}) \mathcal{Z}_A + (\partial_{\theta_g} \lambda_{\mathcal{X}_A}^{\Xi}) \mathcal{X}_A \quad (80)$$

$$+ \frac{1}{2} \sum_{\langle A, A' \rangle} \left(\partial_{\theta_g} \Lambda_{\mathcal{X} \mathcal{X}_{AA'}}^{\Xi} \right) \mathcal{X} \mathcal{X}_{AA'} + \left(\partial_{\theta_g} \Lambda_{\mathcal{Z} \mathcal{Z}_{AA'}}^{\Xi} \right) \mathcal{Z} \mathcal{Z}_{AA'}$$

$$+ \left(\partial_{\theta_g} \Lambda_{\mathcal{Z} \mathcal{X}_{AA'}}^{\Xi} \right) \mathcal{Z} \mathcal{X}_{AA'} + \left(\partial_{\theta_g} \Lambda_{\mathcal{X} \mathcal{Z}_{AA'}}^{\Xi} \right) \mathcal{X} \mathcal{Z}_{AA'}$$

and, by the results from analytical circuit gradients,

$$\partial_{\theta_g} \lambda_{\mathcal{Z}_A}^{\Xi} = \lambda_{\mathcal{Z}_A}^{\Xi, \theta_g + \pi/4} - \lambda_{\mathcal{Z}_A}^{\Xi, \theta_g - \pi/4} \quad (81)$$

Here $\lambda_{\mathcal{Z}_A}^{\Xi, \theta_g + \pi/4}$ is a shorthand to indicate that the Pauli matrix should be reevaluated with all parameters frozen, but with θ_g updated to $\theta_g + \pi/4$.

The sole goal/directive of this subsection is to determine the optimal state-averaged VQE parameters $\{\theta_g^*\}$. The diagonal subspace Hamiltonian matrix elements $H_{\Xi\Xi} \equiv \varepsilon^{\Xi}$ are determined as a side externality of this computation.

6. Technical Detail: VQE Entangler Parametrization

The definition and parametrization of the VQE entangler circuit is something of an art. In any configuration-space basis, the adiabatic eigenfunctions of the real electronic or *ab initio* exciton Hamiltonian can be written as real, orthonormal vectors with arbitrary total phase of ± 1 . Therefore, the VQE entangler operator \hat{U} can be restricted to $SO(2^N)$ without loss. We have previously¹⁴ elected to construct the total VQE entangler circuit for the *ab initio* exciton model by placing a two-body entangler restricted to $SO(4)$ at each two-body interaction site in the exciton Hamiltonian. E.g., for a linear arrangement,



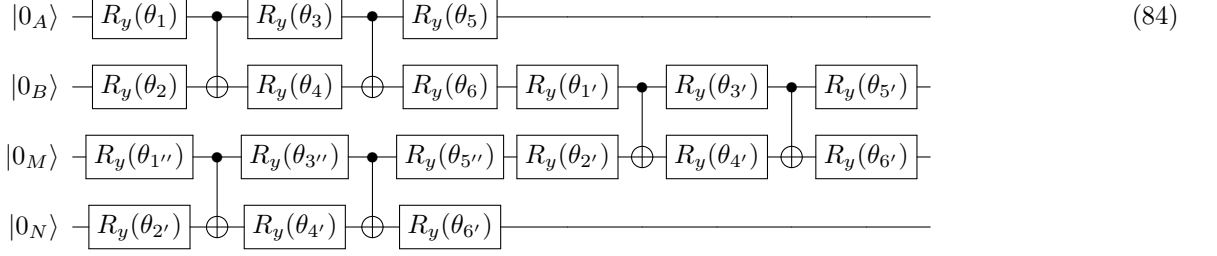
If additional variational flexibility in the ansatz is desired, a straightforward approach is to add additional layers of entanglers of the form shown here, or to extend two-body entanglers to the next layer(s) of nearest neighbors.

We now detail the specific choice of circuit for \hat{U}_2 used to cover $SO(4)$ used in this work. Note that there has been much interest in the literature on the construction of optimal 2-body quantum circuits covering $SU(4)$ or $SO(4)$ using various or arbitrary gate libraries - for an overview, see⁹⁸⁻¹⁰¹. $SO(4)$ is the group of real, orthogonal matrices with determinant +1, and covers all possible two-body entangler matrices needed in our VQE task. There are infinitely many equivalent logical parametrizations of $SO(4)$ with 6 real parameters, but some of these will prove easier to optimize and/or differentiate than others in VQE applications. For today, our selected two-body entangler circuit is¹⁰¹,

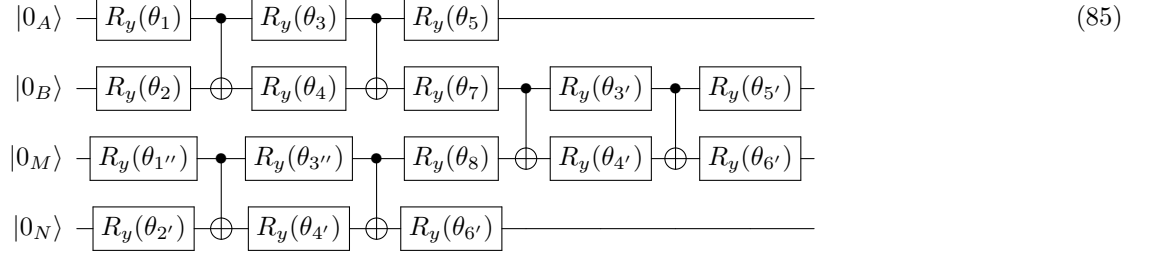
$$\begin{array}{l} |0_A\rangle - [R_y(\theta_1)] - \bullet - [R_y(\theta_3)] - \bullet - [R_y(\theta_5)] \\ |0_B\rangle - [R_y(\theta_2)] - \oplus - [R_y(\theta_4)] - \oplus - [R_y(\theta_6)] \end{array} \quad (83)$$

This circuit was chosen because of its simple representation of parameters in terms of \hat{R}_y gates, which allows for direct implementation of our circuit gradient recipe developed above.

Note that when joining individual $SO(4)$ entangler circuit elements, adjacent \hat{R}_y gates should be merged to minimize the number of VQE parameters and avoid zero eigenvalues of the SA-VQE parameter Hessian (caused by redundancies in the parameters). E.g., for a $N = 4$ linear VQE circuit, the simply adjoined circuit,



should be merged to,



To verify the correctness of the analytical gradients, below we will also use shortened versions of these entangler circuits designed to limit the variational flexibility of the MC-VQE ansatz and to increase the magnitude of the response terms.

7. Subspace Eigenstates

The final MC-VQE eigenstates are determined by solving for the subspace eigenvectors $V_{\Xi\Theta}$ and eigenvalues E_Θ by classically solving the entangled, contracted subspace eigenproblem,

$$\sum_{\Xi'} H_{\Xi\Xi'} V_{\Xi'\Theta} = V_{\Xi\Theta} E_\Theta : \sum_{\Xi} V_{\Xi\Theta} V_{\Xi\Theta'} = \delta_{\Theta\Theta'} \quad (86)$$

where the entangled, contracted subspace Hamiltonian is,

$$H_{\Xi\Xi'} \equiv \langle \Phi_{\Xi} | \hat{U}_{\text{VQE}}^\dagger \hat{H} \hat{U}_{\text{VQE}} | \Phi_{\Xi'} \rangle \quad (87)$$

This can be evaluated by partial tomography measurements on a quantum computer.

$$2H_{\Xi\Xi'} = (\langle \Phi_{\Xi} | + \langle \Phi_{\Xi'} |) \hat{U}_{\text{VQE}}^\dagger \hat{H} \hat{U}_{\text{VQE}} (|\Phi_{\Xi}\rangle + |\Phi_{\Xi'}\rangle) / 2 \\ - (\langle \Phi_{\Xi} | - \langle \Phi_{\Xi'} |) \hat{U}_{\text{VQE}}^\dagger \hat{H} \hat{U}_{\text{VQE}} (|\Phi_{\Xi}\rangle - |\Phi_{\Xi'}\rangle) / 2 \quad (88)$$

$$= \langle \chi_{\Xi\Xi'}^+ | \hat{U}_{\text{VQE}}^\dagger \hat{H} \hat{U}_{\text{VQE}} | \chi_{\Xi\Xi'}^+ \rangle - \langle \chi_{\Xi\Xi'}^- | \hat{U}_{\text{VQE}}^\dagger \hat{H} \hat{U}_{\text{VQE}} | \chi_{\Xi\Xi'}^- \rangle$$

where the ‘‘interfering’’ contracted reference states are,

$$|\chi_{\Xi\Xi'}^\pm\rangle \equiv \sum_I |I\rangle \chi_{I\Xi\Xi'}^\pm \equiv \sum_I |I\rangle \frac{1}{\sqrt{2}} [C_{I\Xi} \pm C_{I\Xi'}] \quad (89)$$

i.e., modified CIS states which can be prepared by the usual CIS state preparation circuits with modified angles.

The procedure to determine the subspace Hamiltonian matrix elements and subspace eigenstates is as follows: Define the ‘‘interfering’’ contracted reference state coefficients as,

$$\chi_{I\Xi\Xi'}^\pm \equiv \frac{1}{\sqrt{2}} [C_{I\Xi} \pm C_{I\Xi'}] \quad \forall \Xi > \Xi' \quad (90)$$

Define the corresponding CIS state preparation circuit angles,

$$\theta_M[\chi_{I\Xi\Xi'}^\pm] \quad (91)$$

Compute the off-diagonal VQE-entangled contracted subspace Hamiltonian elements,

$$H_{\Xi\Xi'} = H_{\Xi'\Xi} = (\varepsilon[\theta_g, \theta_M[\chi_{I\Xi\Xi'}^+]] \quad (92)$$

$$- \varepsilon[\theta_g, \theta_M[\chi_{I\Xi\Xi'}^-]]) / 2 \quad \forall \Xi > \Xi'$$

Note that the diagonal subspace Hamiltonian matrix elements are available from the state-averaged VQE optimization step above. Finally, classically diagonalize the subspace Hamiltonian to determine the subspace eigenvectors $V_{\Xi\Theta}$ and MC-VQE eigenvalues E_Ξ ,

$$\sum_{\Xi'} H_{\Xi\Xi'} V_{\Xi'\Theta} = V_{\Xi\Theta} E_\Theta : \sum_{\Xi} V_{\Xi\Theta} V_{\Xi\Theta'} = \delta_{\Theta\Theta'} \quad (93)$$

8. Generating State Coefficients

For convenience, the MC-VQE states can be re-expressed in terms of ‘‘generating states’’ $|\Gamma_\Theta\rangle$,

$$|\Psi_\Theta\rangle \equiv \hat{U}_{\text{VQE}} |\Gamma_\Theta\rangle \quad (94)$$

where,

$$|\Gamma_\Theta\rangle \equiv \sum_I |I\rangle \Gamma_{I\Theta} \quad (95)$$

where,

$$\Gamma_{I\Theta} \equiv \sum_{\Xi} C_{I\Xi} V_{\Xi\Theta} \quad (96)$$

Thus the generating states are rotations of the contracted reference states, and can also be expressed in CIS form.

To utilize this expression, classically form the ‘‘generating state coefficients,’’

$$\Gamma_{I\Theta} \equiv \sum_{\Xi} C_{I\Xi} V_{\Xi\Theta} \quad (97)$$

And then define the corresponding CIS state preparation circuit angles,

$$\theta_M[\Gamma_{I\Theta}] \quad (98)$$

As a check, one should find,

$$E_\Theta = \varepsilon[\theta_g, \theta_M[\Gamma_{I\Theta}]] \quad (99)$$

C. Quantum MC-VQE Gradient Stage

1. Formal Definition: MC-VQE Energy Gradient and Lagrangian

Pauli-Basis Density Matrices: For a given MC-VQE wavefunction $|\Psi_\Theta\rangle$, the adiabatic state energy is,

$$E_\Theta \equiv \langle \Psi_\Theta | \hat{H} | \Psi_\Theta \rangle \quad (100)$$

and our objective in this section is to form the ‘‘relaxed’’ one- and two-particle density matrices in the Pauli basis, e.g.,

$$\gamma_{Z_A}^\Theta \equiv \frac{dE_\Theta}{dZ_A}, \quad \forall A \quad (101)$$

$$\Gamma_{ZZ_{AA'}}^\Theta \equiv \frac{dE_\Theta}{dZ_{AA'}}, \quad \forall A, A' \in \langle A, A' \rangle \quad (102)$$

Once these are obtained, the total energy gradients can be obtained in the classical portion of the algorithm by the chain rule,

$$\begin{aligned} d_\zeta E_\Theta &= \mathcal{E}^\zeta + \sum_A Z_A^\zeta \gamma_{Z_A}^\Theta + \mathcal{X}_A^\zeta \gamma_{\mathcal{X}_A}^\Theta \\ &+ \frac{1}{2} \sum_{\langle A, A' \rangle} \mathcal{X}_{AA'}^\zeta \Gamma_{\mathcal{X}_{AA'}}^\Theta + \mathcal{Z}_{AA'}^\zeta \Gamma_{\mathcal{Z}_{AA'}}^\Theta \\ &+ \mathcal{Z}_{AA'}^\zeta \Gamma_{\mathcal{Z}_{AA'}}^\Theta + \mathcal{Z}_{AA'}^\zeta \Gamma_{\mathcal{Z}_{AA'}}^\Theta. \end{aligned} \quad (103)$$

Where, e.g., $Z_A^\zeta \equiv d_\zeta Z_A$ is the gradient of the matrix element Z_A with respect to ζ , which can be determined in a final, classical step (itself requiring classical response theory). Note that this gradient always appears contracted with a density matrix quantity, which can often be used to improve efficiency.

The ‘‘unrelaxed’’ one- and two-particle density matrices are, e.g.,

$$\gamma_{Z_A}^{\Theta,0} \equiv \frac{\partial E_\Theta}{\partial Z_A} = \langle \Psi_\Theta | \hat{Z}_A | \Psi_\Theta \rangle, \quad \forall A \quad (104)$$

$$\begin{aligned} \Gamma_{ZZ_{AA'}}^{\Theta,0} &\equiv \frac{\partial E_\Theta}{\partial Z_{AA'}} = \langle \Psi_\Theta | \hat{Z}_A \otimes \hat{Z}_{A'} | \Psi_\Theta \rangle, \\ &\forall A, A' \in \langle A, A' \rangle \end{aligned} \quad (105)$$

These carry the Hellmann-Feynman contributions to the gradient, but are missing the MC-VQE wavefunction response contributions.

MC-VQE Quantum Lagrangian: The corresponding Lagrangian has subspace eigenstate, state-averaged VQE entangler, and contracted reference state constraint terms,

$$\mathcal{L}_\Theta = E_\Theta + \underbrace{\mathcal{L}_\Theta^{\text{SE}} + \mathcal{L}_\Theta^{\text{VQE}} + \mathcal{L}_\Theta^{\text{CRS}}}_0 \quad (106)$$

Here, the subspace eigenstate (SE) Lagrangian contribution is,

$$\begin{aligned} \mathcal{L}_\Theta^{\text{SE}} &\equiv \sum_{\Xi' \Theta'} \tilde{\Xi}_{\Xi' \Theta'}^\Theta \left[\underbrace{\sum_{\Xi''} H_{\Xi' \Xi''} V_{\Xi'' \Theta'} - V_{\Xi' \Theta'} E_{\Theta'}}_{\partial E_{\Theta'} / \partial V_{\Xi' \Theta'} \equiv R_{\Xi' \Theta'}} \right] \\ &: E_\Theta \equiv \sum_{\Xi} \sum_{\Xi'} V_{\Xi\Theta} H_{\Xi\Xi'} V_{\Xi' \Theta} \end{aligned} \quad (107)$$

The state-averaged VQE Lagrangian contribution is,

$$\mathcal{L}_\Theta^{\text{VQE}} \equiv \sum_g \tilde{\theta}_g^\Theta \frac{\partial \bar{E}}{\partial \theta_g} \quad (108)$$

The contracted reference state (CRS) Lagrangian contribution is,

$$\begin{aligned} \mathcal{L}_\Theta^{\text{CRS}} &\equiv \sum_I \sum_{\Xi} \tilde{\Xi}_{I\Xi}^\Theta \left[\underbrace{\sum_{I'} H_{II'} C_{I'\Xi} - C_{I\Xi} E_\Xi^{\text{CIS}}}_{\partial E_\Xi^{\text{CIS}} / \partial C_{I\Xi} \equiv R_{I\Xi}} \right] \\ &: E_\Xi^{\text{CIS}} \equiv \sum_I \sum_{I'} C_{I\Xi} H_{II'} C_{I'\Xi} \end{aligned} \quad (109)$$

Note the nesting of parametric dependencies in the various Lagrangian contributions,

$$E_\Theta(V_{\Xi\Theta}, \theta_g, C_{I\Xi}) \quad (110)$$

$$\mathcal{L}_\Theta^{\text{SE}}(V_{\Xi\Theta}, \theta_g, C_{I\Xi}) \quad (111)$$

$$\mathcal{L}_\Theta^{\text{VQE}}(\theta_g, C_{I\Xi}) \quad (112)$$

$$\mathcal{L}_\Theta^{\text{CRS}}(C_{I\Xi}) \quad (113)$$

This nesting is ubiquitous in Lagrangian approaches to analytical derivative theory. When determining the base quantity E_Θ , we start at the right side of the Lagrangian and work left. When determining the gradient E_Θ^ζ , we start at the left side of the Lagrangian and work right.

2. Subspace Eigenstate Response (Analytical)

The subspace eigenstate response equations have an analytical solution that yields a trivial result for the special case of energy gradients. However, it is still useful to explicitly demonstrate this, as nonzero responses arise from this term for other properties such as non-adiabatic coupling vectors.

The subspace eigenstate response equations are,

$$\frac{\partial \mathcal{L}_\Theta}{\partial V_{\Xi'\Theta'}} = 0 \quad \forall \Xi', \Theta' \quad (114)$$

The “driver” term is,

$$E_\Theta \equiv \sum_{\Xi} \sum_{\Xi'} V_{\Xi\Theta} H_{\Xi\Xi'} V_{\Xi'\Theta} \quad (115)$$

The gradient is,

$$\begin{aligned} G_{\Xi'\Theta'}^\Theta &\equiv \frac{\partial E_\Theta}{\partial V_{\Xi'\Theta'}} = 2 \sum_{\Xi''} H_{\Xi'\Xi''} V_{\Xi''\Theta'} \delta_{\Theta'\Theta} \\ &= 2V_{\Xi'\Theta'} E_{\Theta'} \delta_{\Theta'\Theta} \end{aligned} \quad (116)$$

The Hessian is,

$$\mathcal{H}_{\Xi'\Theta', \Xi''\Theta''} \equiv \frac{\partial^2 E_\Theta}{\partial V_{\Xi'\Theta'} \partial V_{\Xi''\Theta''}} \quad (117)$$

$$= \delta_{\Theta'\Theta''} [H_{\Xi'\Xi''} - E_{\Theta'} (\delta_{\Xi'\Xi''} + 2V_{\Xi'\Theta'} V_{\Xi''\Theta'})]$$

Note that the Hessian is block diagonal in Θ and that the only nonzero gradient term is in the specific state Θ . Therefore, we will only need to solve the subspace eigenstate response equations in the specific state Θ .

The subspace eigenstate response equations (for state Θ) are,

$$\sum_{\Xi'} \mathcal{H}_{\Xi\Theta, \Xi'\Theta} \tilde{\Xi}_{\Xi'\Theta}^\Theta = -G_{\Xi\Theta}^\Theta \quad (118)$$

By inspection (e.g., substitute into the above), the analytical solution is,

$$\tilde{\Xi}_{\Xi\Theta}^\Theta = V_{\Xi\Theta} \quad (119)$$

Therefore, the subspace eigenstate response contribution is,

$$\begin{aligned} \mathcal{L}_\Theta^{\text{SE}} &\equiv \sum_{\Xi} \tilde{\Xi}_{\Xi\Theta}^\Theta \left[\sum_{\Xi'} H_{\Xi\Xi'} V_{\Xi'\Theta} - V_{\Xi\Theta} E_\Theta \right] \\ &= E_\Theta - E_\Theta = \boxed{0} \end{aligned} \quad (120)$$

Note that we are able to write the final zero in this context only because the resultant Lagrangian quantity is absolutely zero in the sense that it and all possible derivatives are zero.

Therefore, we can entirely ignore contributions from $\mathcal{L}_\Theta^{\text{SE}}$ for the rest of the derivation of the energy gradient.

3. Unrelaxed Pauli Density Matrices

Form the unrelaxed Pauli density matrices, e.g.,

$$\gamma_{Z_A}^{\Theta,0} \equiv \frac{\partial E_\Theta}{\partial Z_A} = \lambda_{Z_A} [\theta_g, \theta_M [\Gamma_{I\Theta}]] \quad (121)$$

$$\Gamma_{Z_Z AB}^{\Theta,0} \equiv \frac{\partial E_\Theta}{\partial Z_Z AB} = \Lambda_{Z_Z AB} [\theta_g, \theta_M [\Gamma_{I\Theta}]] \quad (122)$$

4. CP-SA-VQE Response

The coupled-perturbed state-averaged variational quantum eigensolver equations (CP-SA-VQE) are,

$$\frac{\partial \mathcal{L}_\Theta}{\partial \theta_g} = 0 \quad \forall g \quad (123)$$

Both the right- and left-hand-sides of the CP-SA-VQE equations involve quantities from quantum tomography measurements.

5. CP-SA-VQE Response RHS

Form the gradient of the energy with respect to VQE parameters,

$$G_g^\Theta \equiv \frac{\partial E_\Theta}{\partial \theta_g} = \varepsilon^{\theta_g + \pi/4} [\theta_g, \theta_M [\Gamma_{I\Theta}]] \quad (124)$$

$$-\varepsilon^{\theta_g - \pi/4} [\theta_g, \theta_M [\Gamma_{I\Theta}]]$$

6. CP-SA-VQE Response LHS

Form the SA-VQE Hessian, including the diagonal,

$$\mathcal{H}_{gg} \equiv \frac{\partial^2 \bar{E}}{\partial \theta_g^2} = \frac{1}{N_\Theta} \sum_{\Theta} \varepsilon^{\theta_g + \pi/2} [\theta_g, \theta_M [C_{I\Theta}]]$$

$$\begin{aligned}
& +2\varepsilon^{\theta_g}[\theta_g, \theta_M[C_{I\Theta}]] \\
& -\varepsilon^{\theta_g-\pi/2}[\theta_g, \theta_M[C_{I\Theta}]] \quad (125)
\end{aligned}$$

and off-diagonal contributions,

$$\begin{aligned}
\mathcal{H}_{g \neq g'} & \equiv \frac{\partial^2 \bar{E}}{\partial \theta_g \partial \theta_{g'}} = \frac{1}{N_\Theta} \sum_{\Theta} \varepsilon^{\theta_g + \pi/4, \theta_{g'} + \pi/4} [\theta_g, \theta_M[C_{I\Theta}]] \\
& -\varepsilon^{\theta_g + \pi/4, \theta_{g'} - \pi/4} [\theta_g, \theta_M[C_{I\Theta}]] \\
& -\varepsilon^{\theta_g - \pi/4, \theta_{g'} + \pi/4} [\theta_g, \theta_M[C_{I\Theta}]] \\
& +\varepsilon^{\theta_g - \pi/4, \theta_{g'} - \pi/4} [\theta_g, \theta_M[C_{I\Theta}]] \quad (126)
\end{aligned}$$

7. CP-SA-VQE Response Equations

Solve the CP-SA-VQE response equations,

$$\sum_{g'} \mathcal{H}_{gg'} \tilde{\theta}_{g'}^\Theta = -G_g^\Theta \quad (127)$$

8. CP-SA-VQE Response Contribution

The CP-SA-VQE response contribution to the Pauli density matrix is, e.g.,

$$\gamma_{\mathcal{Z}_A}^{\Theta, \text{VQE}} = \sum_g \tilde{\theta}_g \frac{\partial^2 \bar{E}}{\partial \theta_g \partial \mathcal{Z}_A} = \frac{1}{N_\Theta} \sum_{\Theta} \sum_g \tilde{\theta}_g \quad (128)$$

$$\begin{aligned}
& \left[\lambda_{\mathcal{Z}_A}^{\theta_g + \pi/4} [\theta_g, \theta_M[C_{I\Theta}]] \right. \\
& \left. - \lambda_{\mathcal{Z}_A}^{\theta_g - \pi/4} [\theta_g, \theta_M[C_{I\Theta}]] \right]
\end{aligned}$$

9. CP-CRS Response

The coupled-perturbed contracted reference state (CP-CRS) equations are,

$$\frac{\partial \mathcal{L}_\Theta}{\partial C_{I\Xi}} = 0 \quad \forall I, \Xi \quad (129)$$

The right-hand-side of the CP-CRS equations involves quantities from quantum tomography measurements - the left-hand-side is a classical coupled-perturbed configuration interaction singles (CP-CIS) Hessian.

10. CP-CRS Response RHS

The CP-CRS RHS is defined as,

$$G_{I\Xi}^\Theta \equiv \frac{\partial E_\Theta}{\partial C_{I\Xi}} + \frac{\partial \mathcal{L}_\Theta^{\text{VQE}}}{\partial C_{I\Xi}} \quad (130)$$

11. CP-CRS Response RHS #1

The first contribution to the CP-CRS RHS involves the derivative of the state energy with respect to the CIS CRS coefficients through the generator state coefficients and angles,

$$\begin{aligned}
G_{I\Xi}^\Theta & \leftarrow \sum_M \frac{\partial E_\Theta}{\partial \theta_M[\Gamma_{I\Theta}]} \frac{\partial \theta_M[\Gamma_{I\Theta}]}{\partial \Gamma_{I\Theta}} \frac{\partial \Gamma_{I\Theta}}{\partial C_{I\Xi}} \\
& = \sum_M \frac{\partial \varepsilon[\theta_g, \theta_M[\Gamma_{I\Theta}]]}{\partial \theta_M[\Gamma_{I\Theta}]} \frac{\partial \theta_M[\Gamma_{I\Theta}]}{\partial \Gamma_{I\Theta}} V_{\Xi\Theta} \quad (131)
\end{aligned}$$

The gradients of the CIS circuit angles with respect to the corresponding CIS coefficients, i.e., $\partial \theta_M / \partial \Gamma_{I\Theta}$ are classically computed by the Jacobian formula in Equation 62.

The gradients of the VQE-entangled CIS contracted reference states with respect to CIS circuit angles, i.e., $\partial \varepsilon / \partial \theta_M$ can be evaluated by analytical circuit gradients, but care must be taken to account for the fact that pairs of \hat{R}_y gates (plus a CZ gate or equivalent) are used to implement the controlled \hat{F}_y gate for CIS circuits as laid out in Equations 53 and 54. The gradient for the reference angle θ_0 is the usual,

$$\frac{\partial \varepsilon}{\partial \theta_0} = \varepsilon^{\theta_0 + \pi/4} - \varepsilon^{\theta_0 - \pi/4} \quad (132)$$

But the gradients the later angles such as θ_{AB} have additional contributions,

$$\begin{aligned}
\frac{\partial \varepsilon}{\partial \theta_{AB}} & = -(\varepsilon^{\theta_{AB}^L + \pi/4} - \varepsilon^{\theta_{AB}^L - \pi/4})/2 \\
& + (\varepsilon^{\theta_{AB}^R + \pi/4} - \varepsilon^{\theta_{AB}^R - \pi/4})/2 \quad (133)
\end{aligned}$$

Where $\theta_{AB}^L \equiv -\theta_{AB}/2$ is the argument to the left-side \hat{R}_y gate, and $\theta_{AB}^R \equiv +\theta_{AB}/2$ is the argument to the right-side \hat{R}_y gate in Equation 54.

12. CP-CRS Response RHS #2

The second contribution to the CP-CRS RHS involves the derivative of the SA-VQE Lagrangian energy with respect to the CIS CRS coefficients,

$$G_{I\Xi}^\Theta \leftarrow \sum_g \sum_M \tilde{\theta}_g^\Theta \frac{\partial^2 \bar{E}}{\partial \theta_g \partial \theta_M[C_{I\Xi}]} \frac{\partial \theta_M[C_{I\Xi}]}{\partial C_{I\Xi}} \quad (134)$$

$$\begin{aligned}
&= \frac{1}{N_\Theta} \sum_g \sum_M \tilde{\theta}_g^\Theta \frac{\partial \varepsilon^{\theta_g + \pi/4}[\theta_g, \theta_M[C_{I\Xi}]]}{\partial \theta_M[C_{I\Xi}]} \frac{\partial \theta_M[C_{I\Xi}]}{\partial C_{I\Xi}} \\
&\quad - \frac{1}{N_\Theta} \sum_g \sum_M \tilde{\theta}_g^\Theta \frac{\partial \varepsilon^{\theta_g - \pi/4}[\theta_g, \theta_M[C_{I\Xi}]]}{\partial \theta_M[C_{I\Xi}]} \frac{\partial \theta_M[C_{I\Xi}]}{\partial C_{I\Xi}}
\end{aligned}$$

This can be evaluated with the analytical CIS circuit gradients and CIS angle Jacobian discussed in the previous section.

13. CP-CRS Response LHS

The CP-CRS Hessian is (block diagonal in CIS eigenstate Θ),

$$\mathcal{H}_{I\Xi, I'\Xi'} = \delta_{\Xi\Xi'} [H_{II'} - E_\Xi^{\text{CIS}} (\delta_{II'} + 2C_{I\Xi}C_{I'\Xi})] \quad (135)$$

14. CP-CRS Response Equations

Solve the CP-CRS response equations (block diagonal in CIS eigenstate Ξ),

$$\mathcal{H}_{I\Xi, I'\Xi'} \tilde{\Xi}_{I'\Xi'}^\Theta = -G_{I\Xi}^\Theta \quad (136)$$

15. CP-CRS Response Contribution

The CRS response contribution to the density matrix is, e.g.,

$$\begin{aligned}
\gamma_{\mathcal{Z}_A}^{\Theta, \text{CRS}} &\equiv \frac{\partial}{\partial \mathcal{Z}_A} \sum_{I\Xi} \tilde{\Xi}_{I\Xi}^\Theta R_{I\Xi} = \sum_{I\Xi} \tilde{\Xi}_{I\Xi}^\Theta \frac{\partial}{\partial \mathcal{Z}_A} R_{I\Xi} \\
&= \sum_{I\Xi} \sum_{I'I''} \tilde{\Xi}_{I\Xi}^\Theta \frac{\partial R_{I\Xi}}{\partial H_{I'I''}} \frac{\partial H_{I'I''}}{\partial \mathcal{Z}_A} \\
&= \sum_{I'I''} D_{I'I''}^\Theta \frac{\partial H_{I'I''}}{\partial \mathcal{Z}_A} \quad (137)
\end{aligned}$$

where,

$$D_{I'I''}^\Theta = \sum_{\Xi} \tilde{\Xi}_{I'\Xi}^\Theta C_{I''\Xi} - \sum_{\Xi} \left[\sum_I \tilde{\Xi}_{I\Xi}^\Theta C_{I\Xi} \right] C_{I'\Xi} C_{I''\Xi} \quad (138)$$

The final partials of the CIS Hamiltonian with respect to the Pauli-basis potential matrix elements, e.g., $\partial_{\mathcal{Z}_A} H_{I'I''}$, are easily formed by differentiating Equations 48 to 51, which are linear in the Pauli basis potential matrix elements.

16. Relaxed Pauli Density Matrices

The target relaxed Pauli density matrices are simply given as the sum of the unrelaxed density matrices plus the individual response contributions, e.g.,

$$\gamma_{\mathcal{Z}_A}^\Theta \equiv \frac{dE_\Theta}{d\mathcal{Z}_A} = \frac{\partial \mathcal{L}_\Theta}{\partial \mathcal{Z}_A} = \gamma_{\mathcal{Z}_A}^{\Theta, 0} + \gamma_{\mathcal{Z}_A}^{\Theta, \text{VQE}} + \gamma_{\mathcal{Z}_A}^{\Theta, \text{CRS}} \quad (139)$$

D. Classical AIEM Gradient Stage

1. Pauli Basis AIEM Gradient

At present, we have the Lagrangian representation,

$$\begin{aligned}
E_\Theta = \mathcal{L}_\Theta = \mathcal{E} &+ \sum_A \mathcal{Z}_A \gamma_{\mathcal{Z}_A}^\Theta + \mathcal{X}_A \gamma_{\mathcal{X}_A}^\Theta \\
&+ \frac{1}{2} \sum_{\langle A, A' \rangle} \mathcal{X} \mathcal{X}_{AA'} \Gamma_{\mathcal{X} \mathcal{X}_{AA'}}^\Theta + \mathcal{X} \mathcal{Z}_{AA'} \Gamma_{\mathcal{X} \mathcal{Z}_{AA'}}^\Theta \\
&+ \mathcal{Z} \mathcal{X}_{AA'} \Gamma_{\mathcal{Z} \mathcal{X}_{AA'}}^\Theta + \mathcal{Z} \mathcal{Z}_{AA'} \Gamma_{\mathcal{Z} \mathcal{Z}_{AA'}}^\Theta \quad (140)
\end{aligned}$$

But, due to the solution of the response equations above, the Lagrangian is fully relaxed in terms of MC-VQE parameters. Therefore,

$$\begin{aligned}
d_\zeta E_\Theta = \partial_\zeta \mathcal{L}_\Theta = \mathcal{E}^\zeta &+ \sum_A \mathcal{Z}_A^\zeta \gamma_{\mathcal{Z}_A}^\Theta + \mathcal{X}_A^\zeta \gamma_{\mathcal{X}_A}^\Theta \\
&+ \frac{1}{2} \sum_{\langle A, A' \rangle} \mathcal{X} \mathcal{X}_{AA'}^\zeta \Gamma_{\mathcal{X} \mathcal{X}_{AA'}}^\Theta + \mathcal{X} \mathcal{Z}_{AA'}^\zeta \Gamma_{\mathcal{X} \mathcal{Z}_{AA'}}^\Theta \\
&+ \mathcal{Z} \mathcal{X}_{AA'}^\zeta \Gamma_{\mathcal{Z} \mathcal{X}_{AA'}}^\Theta + \mathcal{Z} \mathcal{Z}_{AA'}^\zeta \Gamma_{\mathcal{Z} \mathcal{Z}_{AA'}}^\Theta \quad (141)
\end{aligned}$$

Where, e.g., $\mathcal{Z}_A^\zeta \equiv d_\zeta \mathcal{Z}_A$ is the gradient of the matrix element \mathcal{Z}_A with respect to ζ . What remains is to evaluate the derivatives of the classical matrix elements (including any classical response equations) and efficiently assemble the finished analytical derivative $d_\zeta E_\Theta$.

2. Monomer Basis AIEM Gradient

At this point it is advantageous to perform a linear transformation to a monomer-basis matrix element representation of the gradient,

$$\begin{aligned}
d_\zeta E_\Theta = \sum_A \epsilon_H^{A, \zeta} \gamma_H^{A, \Theta} &+ \epsilon_P^{A, \zeta} \gamma_P^{A, \Theta} + \underbrace{\epsilon_T^{A, \zeta} \gamma_T^{A, \Theta}}_0 \\
&+ \frac{1}{2} \sum_{\langle A, A' \rangle} v_{\text{HH}}^{AA', \zeta} \Gamma_{\text{HH}}^{AA', \Theta} + v_{\text{HT}}^{AA', \zeta} \Gamma_{\text{HT}}^{AA', \Theta} + v_{\text{HP}}^{AA', \zeta} \Gamma_{\text{HP}}^{AA', \Theta}
\end{aligned}$$

$$\begin{aligned}
& + v_{\text{TH}}^{AA',\zeta} \Gamma_{\text{TH}}^{AA',\Theta} + v_{\text{TT}}^{AA',\zeta} \Gamma_{\text{TT}}^{AA',\Theta} + v_{\text{TP}}^{AA',\zeta} \Gamma_{\text{TP}}^{AA',\Theta} \\
& + v_{\text{PH}}^{AA',\zeta} \Gamma_{\text{PH}}^{AA',\Theta} + v_{\text{PT}}^{AA',\zeta} \Gamma_{\text{PT}}^{AA',\Theta} + v_{\text{PP}}^{AA',\zeta} \Gamma_{\text{PP}}^{AA',\Theta} \quad (142)
\end{aligned}$$

Here, the monomer-basis density matrices are defined as, e.g.,

$$\begin{aligned}
\gamma_{\text{H}}^{A'',\Theta} & \equiv \frac{\partial}{\partial \epsilon_{\text{H}}^{A''}} \mathcal{L}_{\Theta} = \frac{\partial}{\partial \epsilon_{\text{H}}^{A''}} \left[\mathcal{E} + \sum_A \mathcal{Z}_A \gamma_{\mathcal{Z}_A}^{\Theta} + \dots \right] \\
& = \underbrace{\left[\frac{\partial}{\partial \epsilon_{\text{H}}^{A''}} \mathcal{E} \right]}_{1/2} + \sum_A \underbrace{\left[\frac{\partial}{\partial \epsilon_{\text{H}}^{A''}} \mathcal{Z}_A \right]}_{\delta_{AA''}/2} \gamma_{\mathcal{Z}_A}^{\Theta} + \dots \quad (143)
\end{aligned}$$

The transformation coefficients indicated by underbraces are easily determined by differentiating Equations 34 to 40, which are linear in the monomer-basis potential matrix elements.

3. Dimer Interaction Matrix Element Gradients

At this point, it is advantageous to contract through partial derivatives of the dimer interaction matrix elements to obtain a monomer-property-only representation of the analytical derivative.

$$\begin{aligned}
d_{\zeta} E_{\Theta} & = \sum_A \epsilon_{\text{H}}^{A,\zeta} \gamma_{\text{H}}^{A,\Theta} + \epsilon_{\text{P}}^{A,\zeta} \gamma_{\text{P}}^{A,\Theta} + \underbrace{\epsilon_{\text{T}}^{A,\zeta}}_0 \gamma_{\text{T}}^{A,\Theta} \\
& + \bar{\mu}_{\text{H}}^{A,\zeta} \bar{\eta}_{\text{H}}^{A,\Theta} + \bar{\mu}_{\text{P}}^{A,\zeta} \bar{\eta}_{\text{P}}^{A,\Theta} + \bar{\mu}_{\text{T}}^{A,\zeta} \bar{\eta}_{\text{T}}^{A,\Theta} + \bar{r}_0^{A,\zeta} \bar{\xi}^{\text{A},\Theta} \quad (144)
\end{aligned}$$

The monomer property density matrices are defined as, e.g.,

$$\begin{aligned}
\bar{\eta}_{\text{H}}^{A'',\Theta} & \equiv \frac{\partial}{\partial \bar{\mu}_{\text{H}}^{A''}} \mathcal{L}_{\Theta} = \frac{\partial}{\partial \bar{\mu}_{\text{H}}^{A''}} \frac{1}{2} \sum_{\langle A,A' \rangle} v_{\text{HH}}^{AA'} \Gamma_{\text{HH}}^{AA',\Theta} \dots \\
& = \frac{1}{2} \sum_{\langle A,A' \rangle} \left[\frac{\partial}{\partial \bar{\mu}_{\text{H}}^{A''}} v_{\text{HH}}^{AA'} \right] \Gamma_{\text{HH}}^{AA',\Theta} \dots \quad (145)
\end{aligned}$$

and,

$$\begin{aligned}
\bar{\xi}^{A'',\Theta} & \equiv \frac{\partial}{\partial \bar{r}_0^{A''}} \mathcal{L}_{\Theta} = \frac{\partial}{\partial \bar{r}_0^{A''}} \frac{1}{2} \sum_{\langle A,A' \rangle} v_{\text{HH}}^{AA'} \Gamma_{\text{HH}}^{AA',\Theta} \dots \\
& = \frac{1}{2} \sum_{\langle A,A' \rangle} \left[\frac{\partial}{\partial \bar{r}_0^{A''}} v_{\text{HH}}^{AA'} \right] \Gamma_{\text{HH}}^{AA',\Theta} \dots \quad (146)
\end{aligned}$$

Some needed partials of Equation 19 are,

$$\frac{\partial}{\partial \bar{\mu}_{A''}} v^{AA'} = \left[\frac{\bar{\mu}_{A'}}{r_{AA'}^3} - 3 \frac{(\bar{\mu}_{A'} \cdot \bar{r}_{AA'}) \bar{r}_{AA'}}{r_{AA'}^5} \right] \delta_{AA''}$$

$$+ \left[\frac{\bar{\mu}_A}{r_{AA'}^3} - 3 \frac{(\bar{\mu}_A \cdot \bar{r}_{AA'}) \bar{r}_{AA'}}{r_{AA'}^5} \right] \delta_{A'A''} \quad (147)$$

and,

$$\begin{aligned}
\frac{\partial}{\partial \bar{r}_{A''}^0} v^{AA'} & = \left[-3 \frac{(\bar{\mu}_A \cdot \bar{\mu}_{A'}) \bar{r}_{AA'}}{r_{AA'}^5} \right. \\
& \quad \left. + 15 \frac{(\bar{\mu}_A \cdot \bar{r}_{AA'}) (\bar{\mu}_{A'} \cdot \bar{r}_{AA'}) \bar{r}_{AA'}}{r_{AA'}^7} \right. \\
& \quad \left. - 3 \frac{(\bar{\mu}_{A'} \cdot \bar{r}_{AA'}) \bar{\mu}_A}{r_{AA'}^5} - 3 \frac{(\bar{\mu}_A \cdot \bar{r}_{AA'}) \bar{\mu}_{A'}}{r_{AA'}^5} \right] [\delta_{A'A''} - \delta_{AA''}] \quad (148)
\end{aligned}$$

4. Monomer Property Gradients

Finally, the contraction of the monomer property density matrices with the monomer property nuclear gradients can be performed as indicated in Equation 144. For today's exercise, this is a simple set of multiply-add operations with pre-supplied monomer property gradients (obtained with classical Lagrangian theory in methods like TD-DFT, including classical response equations like CP-KS). However, it is also possible to defer computation of these derivatives until the last possible moment, at which point the monomer property density matrices are known, and can be contracted with the monomer property gradients on the fly. This can reduce the number of classical response equations that must be solved, and can help sieve the classical gradient equations if some of the monomer property density matrices are sparse.

IV. COMPUTATIONAL DETAILS

The MC-VQE+AIEM energy and analytical gradient expressions of Equations 19 through 148 were implemented in our in-house quantum circuit simulator QUASAR. For the purposes of this manuscript, we simulate ideal infinite sampling of Pauli density matrices by contraction of the relevant statevector amplitudes. Ground state properties are computed with Kohn-Sham density functional theory (KS-DFT), excited state properties are computed with time-dependent DFT in the Tamm-Dancoff approximation (TDA-TD-DFT).¹⁰² The excited state and transition dipole moments are computed in the unrelaxed expectation value formalism. Dipole moments are computed at the mass centers of the monomers. Analytical gradients of the ground- and excited-state energies and the ground-state, excited-state and transition dipole moments are computed within a classical Lagrangian approach involving coupled-perturbed configuration interaction (CP-CI) and coupled-perturbed Kohn Sham (CP-KS) equations in the relevant places. These derivative quantities are computed

up front, and are stored for later contraction with the relaxed density matrices emanating from the quantum MC-VQE portion of the algorithm - we do not explore the full Lagrangian approach with delayed computation of classical response in the present work. All classical electronic structure computations are performed in double precision (unless otherwise indicated) within the TERACHEM GPU-accelerated electronic structure package,^{103–105} and all iterative portions of the computations are tightly converged to facilitate comparison of numerical derivative properties.

V. RESULTS AND DISCUSSION

A. Validation: BChl-a Dimer

As implied by the verbosity of the derivation above, analytical derivative theory requires extensive demonstration of validity to eliminate myriad potential sources of mathematical or programmatic errors. To proceed, we consider the case of a small dimer of simplified BChl-a chromophores depicted in Figure 1. We shorten the VQE entangler circuit to only a pair of R_y gates and we consider only two contracted reference states out of a total of three CIS states. This deliberately limits the flexibility and accuracy of the MC-VQE ansatz, and thereby ensures that the contributions from both CP-SA-VQE response and CP-CIS response will be large, providing a stress test that the non-Hellmann-Feynman contributions have been correctly derived and implemented. We then compare the analytical derivatives to second-order symmetric finite difference derivatives in three successive bases: the relaxed Pauli density matrices 139 (the total derivatives of the state energies with respect to perturbations in the Pauli Hamiltonian matrix elements), the monomer property density matrices of Equations 143, 145, and 146 (the total derivatives of the state energies with respect to perturbations in the classical monomer properties), and the full nuclear gradient of Equation 144 (the total derivatives of the state energy with respect to perturbations in the nuclear positions). This pipeline of comparisons allows us to separately verify the gradients of the quantum portions of the MC-VQE method, the gradients of the AIEM-to-Pauli Hamiltonian transformation, and the classical electronic structure gradients.

1. Pauli Density Matrices

Table I compares the deviations of Pauli-basis density matrices computed with different methods and gradient approaches for the ground state and first excited states of BChl-a dimer within the AIEM based on ω PBE($\omega = 0.3$)/6-31G*-D3.^{106,107} The principal finding is that MC-VQE including all response terms [denoted as VQE(Y,Y) in the table] agrees to $\sim 10^{-10}$ with second-order symmetric finite difference with a stepsize

of 10^{-7} a.u. This is the same level of agreement as obtained between the analytical gradient methodology and finite difference within FCI and CIS, and is several orders of magnitude better agreement than is obtained if either CP-SA-VQE or CP-CIS response is neglected in MC-VQE. In fact, inspection of the top three and bottom three rows of the table indicates that the errors induced by neglecting response terms in MC-VQE gradients are of essentially the same order as the intrinsic deviations between different methods.

2. Monomer Property Density Matrices

Table II shows the same analysis as Table I, but now for monomer-property density matrices. The findings are identical - the response-including MC-VQE gradients agree with finite difference to the same order as FCI or CIS, and the errors induced by neglecting response terms in MC-VQE gradients are of essentially the same order as the intrinsic deviations between different methods.

3. Full Nuclear Gradients

Table III shows the same analysis as Table II, but now for the complete nuclear gradients of selected atoms. The very nature of this study highlights the imperative to have efficient analytical gradient methodology where only a minimal number of response equations are solved: obtaining the finite difference gradient for the full system would have necessitated the computation of the classical electronic structure quantities on a 528-point stencil, which is *more computational effort* than will be required in the excited-state dynamics study of the following section. This effort was deemed to be overtly laborious, and so finite-difference spot checks of the gradients were performed for the five selected atoms indicated in the table. The conclusion is the same as in the previous two sections - response-including MC-VQE gradients agree with finite difference to the same order as FCI or CIS, and the errors induced by neglecting response terms in MC-VQE gradients are of essentially the same order as the intrinsic deviations between different methods. In all cases, the analytical gradient methods agree with finite difference to at least one order of magnitude better than if any response terms are neglected. Moreover, most of the remaining deviation between the analytical gradient methodology and the finite difference methodology likely originates from the error in the finite difference stencil. As evidence for this, full analytical nuclear gradients for FCI and CIS were checked between this code and a separate code written by a different author and using a different set of working equations, and were found to agree to $\sim 10^{-15}$. This, together with the fact that the response including monomer property density matrices of Table II achieved a more-substantial $\sim 10^6 \times$ improvement in agreement with finite difference and the fact that the

contraction with the classical electronic structure property gradients between Table II and Table III is identical between FCI, CIS, and MC-VQE, provides a strong indicator that the full MC-VQE gradients are true analytical derivatives of the MC-VQE energy.

Figure 2 shows a visual comparison of nuclear gradients computed with various levels of theory and inclusions of response terms. The key finding of this study is that there are visual deviations between MC-VQE gradients using different levels of completeness of response terms (bottom panel) and that these deviations are of the same scale as the intrinsic deviations between different methods (top panel).

B. Demonstration: Excited State Dynamics

To demonstrate the potential utility of our hybrid quantum/classical methodology, we have performed an adiabatic excited state dynamics simulation of the system shown in Figure 1. The methodology for this study is the same as previously described, except that the basis is reduced to STO-3G and mixed precision computations are used to facilitate computational expediency of the monomer classical electronic structure computations. The dynamics are initiated on S_1 with a randomized initial momentum vector drawn from a Maxwellian distribution at $T = 300$ K (the same initial conditions are used for all methods). The dynamics are propagated using velocity Verlet with a timestep of 20 a.u. (~ 0.5 fs) for 300 timesteps (~ 145 fs). The energy profiles of the dynamics are depicted in Figure 3. Inspection of the top panel shows a rather ordinary adiabatic dynamics energy profile with reasonable energy conservation profile considering the short overall timescale of the dynamics. The bottom panel shows a magnified view of the total energy profile, in this case zeroed to the mean total energy. A highly compelling finding emerges: the energy conservation profiles of FCI, CIS, and MC-VQE with full inclusion of response are essentially coincident to the order of the linewidths (there are some minor deviations apparent if one zooms in), but MC-VQE without response contributions immediately diverges from the other curves and additionally exhibits larger “excursions” at ~ 10 fs and ~ 75 fs. Even though FCI, CIS, and MC-VQE all have intrinsic differences, it seems that the internal self-consistency of their analytical gradients works to promote a highly coincident energy conservation profile. By contrast, MC-VQE without response contributions has a non-self-consistent gradient that manifests as a loosely random perturbing force, leading to an immediate divergence of the corresponding energy conservation profile. The energy excursions experienced by MC-VQE without response are also characteristic of a non-self-consistent gradient, and will likely lead to more-substantive energy conservation problems at longer timescales. While more-flexible VQE entangler circuits will doubtless lead to higher-accuracy MC-VQE solutions, and, therefore,

smaller response contributions, this study highlights the importance of fully self-consistent analytical derivative methodology with complete inclusion of wavefunction response.

C. Larger Systems and Entangler Circuits

It might be reasonable to expect that one could forgo computation of the response terms if a sufficiently flexible VQE entangler circuit were utilized - i.e., in a hypothetical “full MC-VQE” ansatz, the Hellmann-Feynman formula would be exact because the full MC-VQE states would be equivalent to the FCI states, and one could eschew the response computation without loss. Here, we provide a short case study that indicates that this is not generally the case with practically-sized VQE entangler circuits. We consider the case of a linear BChl-a hexamer ($N = 6$), and use both a truncated VQE entangler circuit consisting of a single R_y gate at the end of each qubit wire (analogous to the truncated entangler used for the BChl-a dimer test case above) and a “standard” VQE entangler circuit with $SO(4)$ entanglers between each nearest neighbor as in Equation 85. The results are summarized in Table IV. The top portion of the table shows that the use of the more-powerful standard VQE entangler circuit reduces the error of the observables by $\sim 3 - 5\times$, concordant with a $4.4\times$ reduction in the error in the full MC-VQE gradient in the fourth line of the bottom portion of the table. This improvement moves the MC-VQE results from being negligibly better than CIS with the truncated VQE entangler to substantially better than CIS with the standard VQE entangler. However, the magnitudes of the response terms in MC-VQE do not substantially diminish, as indicated in the first three lines of the bottom portion of the table. In fact, for the standard entangler, the response terms are of the same size or even larger than the discrepancy between MC-VQE and FCI. Clearly, this is just one case study, and a more-thorough analysis is warranted in future work, but these initial results do seem to indicate that the response terms are non-negligible even in larger systems with practically-sized (non-truncated) VQE entangler circuits.

D. Prospects for Iterative Solution of Quantum Response Equations

As mentioned in the introduction, one of the key findings of Lagrangian-based analytical nuclear theory in classical electronic structure is that the nuclear gradient (or other first derivative properties) can generally be formed in effort that is strictly congruent with the effort required to form the original energy - e.g., the formation of the first excited state energy and analytical nuclear gradient of TD-DFT requires roughly double the cost of the formation of only the first excited state energy, irrespective of the system size. In the present work, we have

nearly obtained this goal - in particular the invocation of the Lagrangian formalism naturally led to a single set of response equations to be solved, regardless of the number of nuclear or other derivative perturbations applied, allowing e.g., for tractable production of nuclear gradients with 264 perturbations in BChl-a dimer. However, close inspection of the critical quantum portions of the gradient algorithm developed herein indicates that the number of quantum observables required to form the gradient does rise in a system-size-dependent manner over that required to form the MC-VQE energy (assuming a gradient-based or Jacobi-1 style¹⁰⁸ approach to converge the MC-VQE parameters). The offending terms stem from the present manuscript's prescription to explicitly evaluate the quantum Hessian quantities $\partial^2 \bar{E} / \partial \theta_g \partial \theta_{g'}$ and $\partial^2 \bar{E} / \partial \theta_g \partial \theta_M$ for the CP-SA-VQE LHS of Equation 126 and the CP-CIS RHS of Equation 134, respectively. However, it is important to recognize that these Hessian quantities are not intrinsically important intermediates - all that we require is their action on certain trial vectors. For instance, the mixed VQE-CIS angle Hessian term arises in a contribution to the CP-CIS RHS where the salient intermediate is,

$$\tau_M \equiv \sum_g \tilde{\theta}_g^\Theta \frac{\partial^2 \bar{E}}{\partial \theta_g \partial \theta_M} \quad (149)$$

Additionally, if iterative linear equation solvers such as PCG, DIIS,^{109,110} or GMRES are invoked (as is often done in the solution of response equations in classical electronic structure methods), the relevant quantity from the VQE-VQE angle Hessian term is,

$$\tau_{g'} \equiv \sum_g b_g \frac{\partial^2 \bar{E}}{\partial \theta_g \partial \theta_{g'}} \quad (150)$$

where b_g is an arbitrary (classically known) trial vector. The contracted quantum response primitives of Equations 149 and 150 have thus far resisted an analytical linear-scaling tomography resolution, but they resemble the gradients of directional derivatives of functions with smoothness bounded by the overall sinusoidal support of the N_{θ_g} -dimensional VQE quantum circuit tomography. Therefore, it seems likely that an accurate tomography approach could be used to resolve these primitives with effort that is linear in N_{θ_g} . Such an approach would reduce the effort of forming the full analytical MC-VQE gradient to within a constant prefactor of the underlying MC-VQE energy. Such methodology will be considered in future work.

VI. SUMMARY AND OUTLOOK

We have explored the application of the Lagrangian formalism for analytical derivative theory to the hybrid quantum/classical MC-VQE+AIEM method, with specialization to the analytical nuclear gradient. In particular, we demonstrated that this approach provides for

a clean separation between the quantum and classical portions of the algorithm, with a cost for the quantum portion that is independent of the number of nuclei per AIEM monomer. Within the quantum portions of the algorithms, the Lagrangian formalism initiated the natural emergence of CP-SA-VQE and CP-CIS response equations which must be solved to account for the definitional choices of the SA-VQE and CIS portions of the MC-VQE wavefunction ansatz. We developed quadrature-based tomography methodology to extract the needed gradient and Hessian matrix elements from quantum circuit measurements, and have outlined a key primitive operation to form contractions of the quantum Hessians with known trial vectors which could potentially reduce the cost of the complete analytical MC-VQE gradient to a constant scaling factor over the underlying MC-VQE energy. Within a trial BChl-a dimer system with a truncated VQE entangler circuit, we validated the analytical MC-VQE gradients by comparison to finite difference computations in the Pauli, monomer-property, and nuclear perturbations, using an ideal quantum circuit simulator. We then explored adiabatic excited state dynamics of the same system, and demonstrated the importance of self-consistent nuclear gradients by showing that Hellmann-Feynman-approximated MC-VQE gradients exhibit unphysical energy excursions due to the missing response terms. In systems with more extensive VQE entangler circuits, the absolute accuracy of MC-VQE will definitionally increase, possibly leading to smaller response contributions that might be able to be neglected in certain applications. However, it remains important to have fully exact analytical derivative methodology to characterize the potential errors arising from such situations. Moreover, if the proposed endeavor to develop improved tomography methodology for the observation of quantum Hessian-vector contractions succeeds, the overall analytical derivative methodology will cost only a constant multiple of the underlying energy, so the use of full response-including nuclear gradients should be vastly preferred to the use of Hellmann-Feynman gradients.

The outlook for hybrid quantum/classical derivative methodology is, in our opinion, highly promising. With the present manuscript, most of the known lore on analytical derivative methodology that has been developed over the past few decades has been translated from the classical to the quantum realm. There exist a number of technically straightforward but highly compelling projects to extend the present methodology to other derivative properties such as non-adiabatic coupling vectors, polarizabilities, and optical response properties. There is also a need to explore the use of this methodology within MC-VQE in Hamiltonians beyond AIEM, e.g., in fermionic Hamiltonians. Finally, many practical issues will have to be dealt with when making the jump from an ideal quantum circuit simulator to noisy quantum hardware. These challenges are well worth tackling, given the prospects of performing large-scale non-adiabatic dynamics simulations with hybrid quantum/classical computing

in the near future.

Acknowledgements: This material is based on work partially supported by the U.S. Department of Energy, Office of Science, Office of Advanced Scientific Computing Research (SciDAC) program.

Financial Disclosure: TJM is a cofounder of PETACHEM LLC. RMP and PLM own stock/options in QC WARE CORP.

Note Added: As we were finalizing the numerical tests in the present manuscript, two noteworthy manuscripts appeared on the arXiv that deal with the

topic of nuclear gradients of the energy in hybrid quantum/classical electronic structure algorithms.^{83,84} Both groups demonstrate their respective methodologies in the context of nuclear derivatives of the ground-state energy in the one-dimensional H₂ system - a system for which the Hellmann-Feynman theorem holds for the first derivative for standard VQE, and for which the one-dimensional nature of the system makes explicit forward differentiation of wavefunction response contributions much more tractable than in high-dimensional systems such as those encountered in MC-VQE+AIEM.

* Electronic address: rob.parrish@qcware.com

¹ A. Peruzzo et al., Nat. Comm. **5**, 4213 (2014).

² J. Preskill, Quantum **2**, 79 (2018).

³ J. R. McClean, J. Romero, R. Babbush, and A. Aspuru-Guzik, New J. Phys. **18**, 023023 (2016).

⁴ P. O'Malley et al., Phys. Rev. X **6**, 031007 (2016).

⁵ A. Kandala et al., Nature **549**, 242 (2017).

⁶ J. R. McClean et al., arXiv preprint arXiv:1710.07629 (2017).

⁷ J. Romero et al., Quant. Sci. Tech. **4**, 014008 (2018).

⁸ Y. Nam et al., arXiv preprint arXiv:1902.10171 (2019).

⁹ J. R. McClean, M. E. Kimchi-Schwartz, J. Carter, and W. A. de Jong, Phys. Rev. A **95**, 042308 (2017).

¹⁰ O. Higgott, D. Wang, and S. Brierley, arXiv preprint arXiv:1805.08138 (2018).

¹¹ J. Lee, W. J. Huggins, M. Head-Gordon, and K. B. Whaley, J. Chem. Theory Comput. **15**, 311 (2018).

¹² J. I. Colless et al., Phys. Rev. X **8**, 011021 (2018).

¹³ K. M. Nakanishi, K. Mitarai, and K. Fujii, arXiv preprint arXiv:1810.09434 (2018).

¹⁴ R. M. Parrish, E. G. Hohenstein, P. L. McMahan, and T. J. Martínez, Phys. Rev. Lett. **122**, 230401 (2019).

¹⁵ S. Bratož, Colloq. Int. CNRS **82**, 287 (1958).

¹⁶ J. Gerratt and I. M. Mills, J. Chem. Phys. **49**, 1719 (1968).

¹⁷ P. Pulay, Mol. Phys. **17**, 197 (1969).

¹⁸ S. Kato and K. Morokuma, Chem. Phys. Lett. **65**, 19 (1979).

¹⁹ J. D. Goddard, N. C. Handy, and H. F. Schaefer III, J. Chem. Phys. **71**, 1525 (1979).

²⁰ P. Pulay, G. Fogarasi, F. Pang, and J. E. Boggs, J. Am. Chem. Soc. **101**, 2550 (1979).

²¹ B. R. Brooks et al., J. Chem. Phys. **72**, 4652 (1980).

²² R. Krishnan, H. Schlegel, and J. Pople, J. Chem. Phys. **72**, 4654 (1980).

²³ M. Dupuis, J. Chem. Phys. **74**, 5758 (1981).

²⁴ H. Nakatsuji, T. Hayakawa, and M. Hada, Chem. Phys. Lett. **80**, 94 (1981).

²⁵ H. F. Schaefer III and Y. Yamaguchi, J. Mol. Struct. **135**, 369 (1986).

²⁶ G. H. F. Diercksen, B. O. Roos, and A. J. Sadlej, Chem. Phys. **59**, 29 (1981).

²⁷ J. Almlöf and P. R. Taylor, Int. J. Quant. Chem. **27**, 743 (1985).

²⁸ Y. Yamaguchi, M. Frisch, J. Gaw, H. F. Schaefer, and J. S. Binkley, J. Chem. Phys. **84**, 2262 (1986).

²⁹ M. A. Ball and A. D. McLachlan, Mol. Phys. **7**, 501

(1964).

³⁰ A. D. McLachlan and M. A. Ball, Rev. Mod. Phys. **36**, 844 (1964).

³¹ H. D. Cohen and C. C. J. Roothaan, J. Chem. Phys. **43**, S34 (1965).

³² G. J. B. Hurst, M. Dupuis, and E. Clementi, J. Chem. Phys. **89**, 385 (1988).

³³ R. D. Amos, Chem. Phys. Lett. **124**, 376 (1986).

³⁴ P. Stephens, F. Devlin, C. Chabalowski, and M. J. Frisch, J. Phys. Chem. **98**, 11623 (1994).

³⁵ D. McCann and P. Stephens, J. Org. Chem. **71**, 6074 (2006).

³⁶ T. D. Crawford, M. C. Tam, and M. L. Abrams, J. Phys. Chem. A **111**, 12057 (2007).

³⁷ K. Wolinski, J. F. Hinton, and P. Pulay, J. Am. Chem. Soc. **112**, 8251 (1990).

³⁸ T. A. Keith and R. F. W. Bader, Chem. Phys. Lett. **194**, 1 (1992).

³⁹ T. A. Keith and R. F. W. Bader, Chem. Phys. Lett. **210**, 223 (1993).

⁴⁰ K. Ruud, T. Helgaker, K. L. Bak, P. Jørgensen, and H. J. A. Jensen, J. Chem. Phys. **99**, 3847 (1993).

⁴¹ J. R. Cheeseman, G. W. Trucks, T. A. Keith, and M. J. Frisch, J. Chem. Phys. **104**, 5497 (1996).

⁴² T. Helgaker, M. Jaszuński, and K. Ruud, Chem. Rev. **99**, 293 (1999).

⁴³ C. Ochsenfeld, J. Kussmann, and F. Koziol, Angewandte Chemie International Edition **43**, 4485 (2004).

⁴⁴ V. Sychrovský, J. Gräfenstein, and D. Cremer, J. Chem. Phys. **113**, 3530 (2000).

⁴⁵ T. Helgaker, M. Watson, and N. C. Handy, J. Chem. Phys. **113**, 9402 (2000).

⁴⁶ B. Fernandez et al., J. Chem. Phys. **97**, 3412 (1992).

⁴⁷ J. Pople et al., Int. J. Quant. Chem. **20**, 269 (1981).

⁴⁸ Y. Osamura et al., Chem. Phys. **72**, 131 (1982).

⁴⁹ B. H. Lengsfeld, P. Saxe, and D. R. Yarkony, J. Chem. Phys. **81**, 4549 (1984).

⁵⁰ P. Saxe, B. H. Lengsfeld, and D. R. Yarkony, Chem. Phys. Lett. **113**, 159 (1985).

⁵¹ B. H. Lengsfeld and D. R. Yarkony, J. Chem. Phys. **84**, 348 (1986).

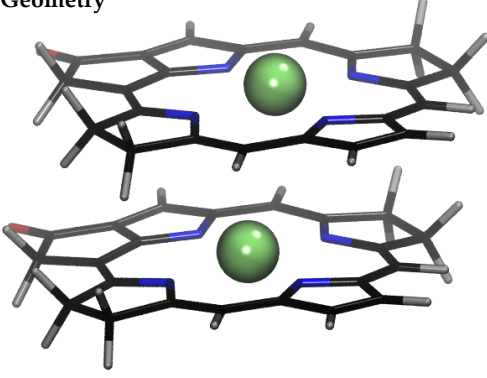
⁵² P. Saxe and D. R. Yarkony, J. Chem. Phys. **86**, 321 (1987).

⁵³ B. H. Lengsfeld and D. R. Yarkony, Adv. Chem. Phys. **82**, 1 (1992).

⁵⁴ A. Sisto, D. R. Glowacki, and T. J. Martinez, Acc. Chem. Res. **47**, 2857 (2014).

- ⁵⁵ A. Sisto et al., *Phys. Chem. Chem. Phys.* **19**, 14924 (2017).
- ⁵⁶ X. Li, R. M. Parrish, F. Liu, S. I. Kokkila Schumacher, and T. J. Martínez, *J. Chem. Theory Comput.* **13**, 3493 (2017).
- ⁵⁷ P. Jørgensen and J. Simons, *Geometrical derivatives of energy surfaces and molecular properties*, volume 166, Springer Science & Business Media, 2012.
- ⁵⁸ G. Mills and H. Jónsson, *Phys. Rev. Lett.* **72**, 1124 (1994).
- ⁵⁹ G. Henkelman, B. P. Uberuaga, and H. Jónsson, *J. Chem. Phys.* **113**, 9901 (2000).
- ⁶⁰ E. Weinan, W. Ren, and E. Vanden-Eijnden, *Phys. Rev. B* **66**, 052301 (2002).
- ⁶¹ B. Peters, A. Heyden, A. T. Bell, and A. Chakraborty, *J. Chem. Phys.* **120**, 7877 (2004).
- ⁶² A. Behn, P. M. Zimmerman, A. T. Bell, and M. Head-Gordon, *J. Chem. Phys.* **135**, 224108 (2011).
- ⁶³ M. Ben-Nun, J. Quenneville, and T. J. Martínez, *J. Phys. Chem. A* **104**, 5161 (2000).
- ⁶⁴ J. C. Tully, *J. Chem. Phys.* **93**, 1061 (1990).
- ⁶⁵ K. Saita and D. V. Shalashilin, *J. Chem. Phys.* **137**, 22A506 (2012).
- ⁶⁶ G. Richings et al., *International Reviews in Physical Chemistry* **34**, 269 (2015).
- ⁶⁷ H. F. Schaefer III and Y. Yamaguchi, *J. Mol. Struct.* **135**, 369 (1986).
- ⁶⁸ N. C. Handy and H. F. Schaefer III, *J. Chem. Phys.* **81**, 5031 (1984).
- ⁶⁹ A. Dalgarno and A. Stewart, *Proceedings of the Royal Society of London. Series A. Mathematical and Physical Sciences* **247**, 245 (1958).
- ⁷⁰ T. U. Helgaker, *Int. J. Quant. Chem.* **21**, 939 (1982).
- ⁷¹ P. Jørgensen and T. Helgaker, *J. Chem. Phys.* **89**, 1560 (1988).
- ⁷² T. Helgaker, P. Jørgensen, and N. C. Handy, *Theoretica chimica acta* **76**, 227 (1989).
- ⁷³ T. Helgaker and P. Jørgensen, *Theoretica chimica acta* **75**, 111 (1989).
- ⁷⁴ T. Helgaker and P. Jørgensen, Calculation of geometrical derivatives in molecular electronic structure theory, in *Methods in Computational Molecular Physics*, pages 353–421, Springer, 1992.
- ⁷⁵ P. G. Szalay, *Int. J. Quant. Chem.* **55**, 151 (1995).
- ⁷⁶ J. Stålring, A. Bernhardsson, and R. Lindh, *Mol. Phys.* **99**, 103 (2001).
- ⁷⁷ K. Hald et al., *J. Chem. Phys.* **118**, 2985 (2003).
- ⁷⁸ S. V. Levchenko, T. Wang, and A. I. Krylov, *J. Chem. Phys.* **122**, 224106 (2005).
- ⁷⁹ S. Coriani et al., *J. Chem. Theory Comput.* **6**, 1028 (2010).
- ⁸⁰ J. Rekkedal et al., *J. Chem. Phys.* **139**, 081101 (2013).
- ⁸¹ I. Kassal and A. Aspuru-Guzik, *J. Chem. Phys.* **131**, 224102 (2009).
- ⁸² A. Roggero and J. Carlson, arXiv preprint arXiv:1804.01505 (2018).
- ⁸³ T. E. O'Brien et al., arXiv e-prints, arXiv:1905.03742 (2019).
- ⁸⁴ K. Mitarai, Y. O. Nakagawa, and W. Mizukami, arXiv e-prints, arXiv:1905.04054 (2019).
- ⁸⁵ P. Jordan and E. Wigner, *Z. Phys.* **47**, 631 (1928).
- ⁸⁶ G. Ortiz, J. E. Gubernatis, E. Knill, and R. Laflamme, *Phys. Rev. A* **64**, 022319 (2001).
- ⁸⁷ S. B. Bravyi and A. Y. Kitaev, *Ann. Phys.* **298**, 210 (2002).
- ⁸⁸ J. T. Seeley, M. J. Richard, and P. J. Love, *J. Chem. Phys.* **137**, 224109 (2012).
- ⁸⁹ K. Setia and J. D. Whitfield, arXiv preprint arXiv:1712.00446 (2017).
- ⁹⁰ K. Setia, S. Bravyi, A. Mezzacapo, and J. D. Whitfield, arXiv preprint arXiv:1810.05274 (2018).
- ⁹¹ R. Babbush et al., arXiv preprint arXiv:1706.00023 (2017).
- ⁹² I. D. Kivlichan et al., *Phys. Rev. Lett.* **120**, 110501 (2018).
- ⁹³ M. Motta et al., arXiv preprint arXiv:1808.02625 (2018).
- ⁹⁴ P. Güttinger, *Zeitschrift für Physik* **73**, 169 (1932).
- ⁹⁵ W. Pauli, *Handbuch der Physik* **24**, 162 (1933).
- ⁹⁶ H. Hellman, *Franz Deuticke, Leipzig*, 285 (1937).
- ⁹⁷ R. P. Feynman, *Phys. Rev.* **56**, 340 (1939).
- ⁹⁸ J. Zhang, J. Vala, S. Sastry, and K. B. Whaley, *Phys. Rev. Lett.* **91**, 027903 (2003).
- ⁹⁹ V. V. Shende, I. L. Markov, and S. S. Bullock, *Phys. Rev. A* **69**, 062321 (2004).
- ¹⁰⁰ F. Vatan and C. Williams, *Phys. Rev. A* **69**, 032315 (2004).
- ¹⁰¹ H.-R. Wei and Y.-M. Di, arXiv preprint arXiv:1203.0722 (2012).
- ¹⁰² E. Runge and E. K. Gross, *Phys. Rev. Lett.* **52**, 997 (1984).
- ¹⁰³ I. S. Ufimtsev and T. J. Martínez, *J. Chem. Theory Comput.* **5**, 2619 (2009).
- ¹⁰⁴ N. Luehr, I. S. Ufimtsev, and T. J. Martínez, *J. Chem. Theory Comput.* **7**, 949 (2011).
- ¹⁰⁵ C. M. Isborn, A. W. Gotz, M. A. Clark, R. C. Walker, and T. J. Martínez, *J. Chem. Theory Comput.* **8**, 5092 (2012).
- ¹⁰⁶ Y. Tawada, T. Tsuneda, S. Yanagisawa, T. Yanai, and K. Hirao, *J. Chem. Phys.* **120**, 8425 (2004).
- ¹⁰⁷ O. A. Vydrov and G. E. Scuseria, *J. Chem. Phys.* **125**, 234109 (2006).
- ¹⁰⁸ R. M. Parrish, J. T. Iosue, A. Ozaeta, and P. L. McMahon, arXiv preprint arXiv:1904.03206 (2019).
- ¹⁰⁹ P. Pulay, *Chem. Phys. Lett.* **73**, 393 (1980).
- ¹¹⁰ P. Pulay, *J. Comp. Chem.* **3**, 556 (1982).

A. Geometry



B. MC-VQE Quantum Circuit

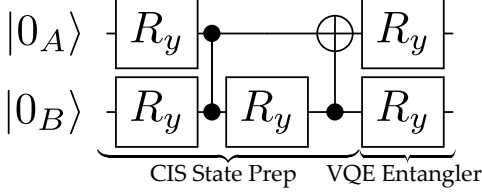
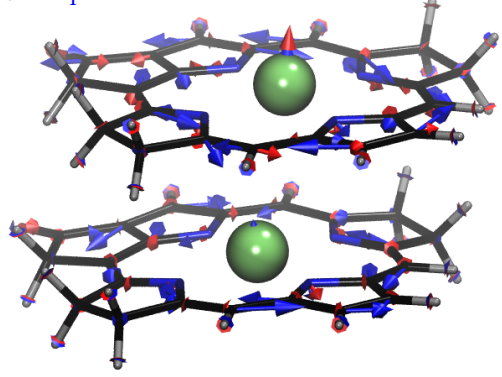
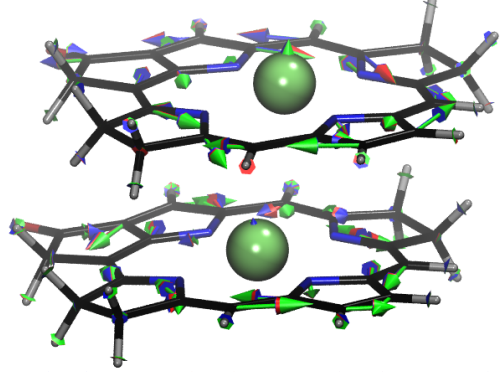


FIG. 1: Schematic of (A) BChl-a dimer system and (B) corresponding truncated MC-VQE quantum circuit selected for analytical gradient validation and excited-state dynamics demonstration in Sections V A and V B. The VQE entangler circuit element is deliberately truncated to limit the flexibility of the ansatz, yielding large wavefunction response contributions.

A. S_0 vs. S_1 Gradients (FCI):



B. FCI vs. CIS vs. VQE(Y,Y) Gradients (S_1):



C. VQE(Y,Y) vs. VQE(Y,N) vs. VQE(N,Y) vs. VQE(N,N) Gradients (S_1):

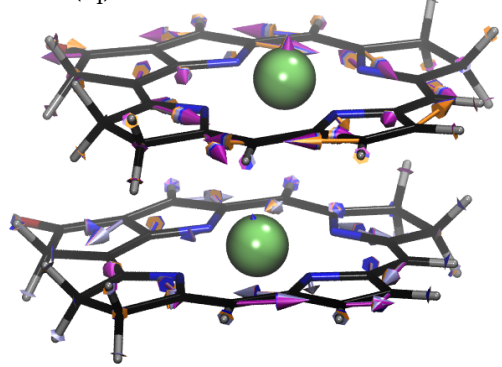


FIG. 2: Visual comparison of nuclear gradients computed for BChl-a dimer within the AIEM based on ω PBE($\omega = 0.3$)/6-31G*-D3. (A) Ground-state [red] vs. first-excited-state [blue] gradients computed with FCI. (B) FCI [blue] vs. CIS [green] vs. VQE [red] gradients computed on S_1 . (C) VQE gradients computed with different inclusion of response terms on S_1 . The notation VQE(N,Y) indicates that VQE response (the first argument) was not used while CIS response (the second argument) was used. For MC-VQE, two states were computed and the VQE entangler circuit of Figure 1 was used.

TABLE I: Comparison of Pauli-basis density matrices computed for BChl-a dimer within the AIEM based on ω PBE($\omega = 0.3$)/6-31G*-D3. The upper portion of the table shows the deviation between the analytical and finite-difference formulations of the Pauli-basis density matrices, with a second-order symmetric finite difference stencil with stepsize of 10^{-7} used for all quantities. The bottom portion of the table shows the deviation between different methods with analytical formulations of the Pauli-basis density matrices. In all cases, the maximum absolute deviation across the ground-state and first-excited-state Pauli density matrices is reported. The notation VQE(N,Y) indicates that VQE response (the first argument) was not used while CIS response (the second argument) was used. For MC-VQE, two states were computed and the VQE entangler circuit of Figure 1 was used.

Method	$\gamma_{\mathcal{X}_A}^\Theta$	$\gamma_{\mathcal{Z}_A}^\Theta$	$\Gamma_{\mathcal{X}\mathcal{X}_{AA'}}^\Theta$	$\Gamma_{\mathcal{X}\mathcal{Z}/\mathcal{Z}\mathcal{X}_{AA'}}^\Theta$	$\Gamma_{\mathcal{Z}\mathcal{Z}_{AA'}}^\Theta$
Analytical vs. Finite Difference					
VQE(N,N)	1.2×10^{-1}	1.2×10^{-1}	5.7×10^{-2}	6.1×10^{-2}	4.0×10^{-2}
VQE(N,Y)	7.0×10^{-2}	1.0×10^{-2}	1.4×10^{-2}	4.0×10^{-2}	1.6×10^{-2}
VQE(Y,N)	5.0×10^{-2}	1.3×10^{-1}	7.1×10^{-2}	5.0×10^{-2}	2.4×10^{-2}
VQE(Y,Y)	3.0×10^{-10}	2.4×10^{-11}	2.6×10^{-11}	2.1×10^{-10}	5.0×10^{-11}
FCI	1.3×10^{-10}	1.7×10^{-10}	1.2×10^{-10}	9.1×10^{-11}	7.6×10^{-11}
CIS	1.5×10^{-10}	1.5×10^{-10}	3.1×10^{-11}	1.5×10^{-10}	9.6×10^{-11}
Method vs. Method (Analytical)					
FCI-VQE	9.4×10^{-2}	3.7×10^{-2}	1.9×10^{-1}	6.7×10^{-2}	2.5×10^{-2}
FCI-CIS	2.3×10^{-1}	1.5×10^{-1}	1.6×10^{-1}	2.4×10^{-1}	3.7×10^{-2}
VQE-CIS	2.0×10^{-1}	1.2×10^{-1}	5.4×10^{-2}	1.8×10^{-1}	2.2×10^{-2}

TABLE II: Comparison of monomer property density matrices computed for BChl-a dimer within the AIEM based on ω PBE($\omega = 0.3$)/6-31G*-D3. The upper portion of the table shows the deviation between the analytical and finite-difference formulations of the monomer property density matrices, with a second-order symmetric finite difference stencil with stepsize of 10^{-7} used for the γ quantities and with stepsize of 10^{-6} used for the $\vec{\eta}$ and $\vec{\zeta}$ quantities. The bottom portion of the table shows the deviation between different methods with analytical formulations of the monomer property density matrices. In all cases, the maximum absolute deviation across the ground-state and first-excited-state monomer property density matrices is reported. The notation VQE(N,Y) indicates that VQE response (the first argument) was not used while CIS response (the second argument) was used. For MC-VQE, two states were computed and the VQE entangler circuit of Figure 1 was used.

Method	$\gamma_H^{A,\Theta}$	$\gamma_T^{A,\Theta}$	$\gamma_P^{A,\Theta}$	$\vec{\eta}_H^{A,\Theta}$	$\vec{\eta}_T^{A,\Theta}$	$\vec{\eta}_P^{A,\Theta}$	$\vec{\zeta}_P^{A,\Theta}$
Analytical vs. Finite Difference							
VQE(N,N)	6.0×10^{-2}	1.2×10^{-1}	6.0×10^{-2}	4.7×10^{-4}	5.0×10^{-4}	3.9×10^{-4}	3.1×10^{-4}
VQE(N,Y)	5.2×10^{-3}	7.0×10^{-2}	5.2×10^{-3}	7.3×10^{-5}	1.9×10^{-4}	3.7×10^{-4}	1.3×10^{-4}
VQE(Y,N)	6.3×10^{-2}	5.0×10^{-2}	6.3×10^{-2}	4.4×10^{-4}	4.5×10^{-4}	3.8×10^{-4}	3.0×10^{-4}
VQE(Y,Y)	2.0×10^{-10}	1.6×10^{-10}	1.7×10^{-10}	4.0×10^{-11}	3.3×10^{-11}	3.9×10^{-11}	2.1×10^{-11}
FCI	8.4×10^{-11}	1.3×10^{-10}	7.3×10^{-11}	1.3×10^{-11}	1.4×10^{-11}	2.3×10^{-11}	3.4×10^{-11}
CIS	4.0×10^{-11}	1.5×10^{-10}	6.4×10^{-11}	2.6×10^{-11}	9.0×10^{-12}	1.6×10^{-11}	1.6×10^{-11}
Method vs. Method (Analytical)							
FCI-VQE	1.9×10^{-2}	9.4×10^{-2}	1.9×10^{-2}	2.3×10^{-4}	1.2×10^{-3}	4.6×10^{-4}	1.2×10^{-3}
FCI-CIS	7.7×10^{-2}	2.3×10^{-1}	7.7×10^{-2}	4.0×10^{-4}	1.2×10^{-3}	1.6×10^{-3}	1.7×10^{-3}
VQE-CIS	5.8×10^{-2}	2.0×10^{-1}	5.8×10^{-2}	3.3×10^{-4}	8.8×10^{-4}	1.3×10^{-3}	1.1×10^{-3}

TABLE III: Comparison of nuclear gradients computed for BChl-a dimer within the AIEM based on ω PBE($\omega = 0.3$)/6-31G*-D3. The upper portion of the table shows the deviation between the analytical and finite-difference formulations of the monomer property density matrices, with a second-order symmetric finite difference stencil with stepsize of 0.002 Å. The bottom portion of the table shows the deviation between different methods with analytical formulations of the nuclear gradients. In all cases, the maximum absolute deviation across the ground-state and first-excited-state monomer nuclear gradients is reported. The notation VQE(N,Y) indicates that VQE response (the first argument) was not used while CIS response (the second argument) was used. For MC-VQE, two states were computed and the VQE entangler circuit of Figure 1 was used. The notation Mg_A^{20} indicates that the comparison is over the x , y , and z components of the nuclear gradient on the Mg atom at index 20 (zero-based) on monomer A .

Method	Mg_A^{20}	O_A^{41}	N_A^{16}	C_B^{22}	H_B^{31}
Analytical vs. Finite Difference					
VQE(N,N)	7.5×10^{-4}	1.4×10^{-3}	1.1×10^{-3}	1.8×10^{-3}	2.7×10^{-5}
VQE(N,Y)	4.0×10^{-4}	7.1×10^{-4}	1.3×10^{-3}	1.1×10^{-3}	2.0×10^{-5}
VQE(Y,N)	3.5×10^{-4}	7.1×10^{-4}	1.1×10^{-3}	2.9×10^{-3}	4.6×10^{-5}
VQE(Y,Y)	6.3×10^{-7}	5.5×10^{-6}	2.2×10^{-6}	2.5×10^{-6}	1.3×10^{-6}
FCI	6.3×10^{-7}	5.5×10^{-6}	2.4×10^{-6}	2.5×10^{-6}	1.3×10^{-6}
CIS	6.2×10^{-7}	5.5×10^{-6}	1.9×10^{-6}	2.5×10^{-6}	1.3×10^{-6}
Method vs. Method (Analytical)					
FCI-VQE	5.7×10^{-4}	9.6×10^{-4}	1.0×10^{-3}	5.8×10^{-4}	2.2×10^{-5}
FCI-CIS	1.7×10^{-3}	2.9×10^{-3}	5.3×10^{-3}	7.6×10^{-4}	2.0×10^{-5}
VQE-CIS	1.5×10^{-3}	2.5×10^{-3}	4.3×10^{-3}	3.2×10^{-4}	1.3×10^{-5}

TABLE IV: Comparison of nuclear gradients computed for BChl-a hexamer ($N = 6$) within AIEM based on ω PBE($\omega = 0.3$)/6-31G*-D3. The upper portion of the table shows the errors of the MC-VQE energy and oscillator strength observables vs. FCI. The lower portion of the table shows the maximum absolute deviations between various analytical gradient methods for the first excited state nuclear energy gradient. The first column of data shows the results from a truncated VQE entangler with a single R_y gate at the end of each qubit wire, analogous to the truncated VQE entangler used for the BChl-a dimer example in the rest of the manuscript. The second column of data shows the results from a full $SO(4)$ entangler of Equation 85.

Method	1-Layer	5-Layer
Accuracy Characteristics		
E^0	5.4×10^{-3}	7.6×10^{-4}
E^1	3.9×10^{-3}	5.7×10^{-4}
$\Delta E^{0 \rightarrow 1}$	1.4×10^{-3}	1.9×10^{-4}
$O^{0 \rightarrow 1}$	1.5×10^{-4}	5.9×10^{-5}
Gradient Deviations		
VQE(Y,Y)-VQE(N,N)	1.2×10^{-3}	1.7×10^{-3}
VQE(Y,Y)-VQE(N,Y)	2.4×10^{-3}	1.5×10^{-3}
VQE(Y,Y)-VQE(Y,N)	1.2×10^{-3}	7.5×10^{-4}
FCI-VQE(Y,Y)	4.9×10^{-3}	1.1×10^{-3}
FCI-CIS	8.5×10^{-3}	8.5×10^{-3}
VQE(Y,Y)-CIS	3.6×10^{-3}	7.5×10^{-3}

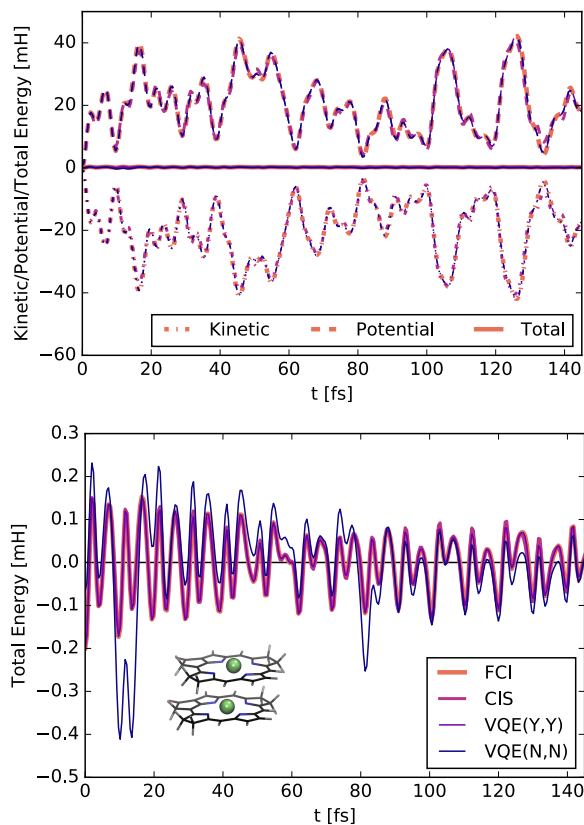


FIG. 3: Energy characteristics of S_1 adiabatic excited-state dynamics of BChl-a dimer within the AIEM based on ω PBE($\omega = 0.3$)-D3/STO-3G, computed using velocity Verlet with a timestep of 20 au (~ 0.5 fs) and analytical nuclear gradients. Top panel: Kinetic, potential, and total energy profiles, all zeroed to the values at the initial frame. Bottom panel: magnified view of the total energy profile from the top panel, zeroed to the mean total energy. The notation VQE(N,Y) indicates that VQE response (the first argument) was not used while CIS response (the second argument) was used. For MC-VQE, two states were computed and the VQE entangler circuit of Figure 1 was used.